Research Article

Vibration Response of a Sandwich Higher-Order Micro Beam based on Shear and Normal Deformation Theory on Kerr Elastic Foundation with Thickness Stretching Effect

Seyed Amir Sajadian ⓘ, Mehdi Mohammadimehr* ⓘ, Mohsen Irani Rahaghi ⓘ

Department of Solid Mechanics, Faculty of Mechanical Engineering, University of Kashan, Ghotb Ravandi Blvd., Kashan, Iran

ARTICLE INFO

ABSTRACT

The novelty of this study is to consider the vibration analysis of a sandwich structure using shear and normal deformation beam theory (SNDBT) with a porous core and various reinforcement materials, including carbon nanorods (CNRs), graphene platelets (GPLs), and carbon nanotubes (CNTs), by considering the size effect based on modified couple stress theory (MCST) or nonlocal strain gradient theory (NSGT) on various elastic foundation such as Winkler, Pasternak, and Kerr, simultaneously. Also, each layer in the microbeam has different mechanical properties as a function of temperature. The governing equations of motion are derived using Hamilton's principle and the energy approach by considering the variational method, and then these equations are solved using Navier's method. The results are compared with those recently published by other scientists. The purpose of this study is to present a comprehensive and efficient innovative analytical framework for understanding the vibration behavior of a sandwich microbeams with different cores and reinforcements, and types of elastic foundations. In the higher-order shear and normal deformation theory by applying the stretching functions, the proposed model offers advantages that can increase the computational efficiency. In addition, a comprehensive parametric study is carried out to evaluate the effect of various properties, including porosity distributions, small-scale parameters, different elastic foundations, thickness, axial wave number, small-scale theories, volume fraction, and different reinforcements such as GPLs, CNTs, and CNRs. It is concluded that GPLs have the highest frequency, and CNRs have the lowest frequency. Also, by increasing the volume fraction of the reinforcements, the natural frequency of the sandwich microbeam increases for GPLs by 10%, the CNTs by 7%, and the CNRs by 4%. The current study shows that the considering of an elastic foundation for a beam has been demonstrated to result in an increase in the frequencies. Furthermore, the results with and without the thickness stretching effect show that the shear and normal beam theory improves the results. The natural frequency increases by 67.4%, when FG-XX is compared to FG-UU face sheets. It decreases by 24.8% when FG-OO is compared to FG-UU. The sandwich beams are compared to those without reinforcement.

* Corresponding author.
   E-mail address: mmohammadimehr@kashanu.ac.ir

1. Introduction

Composite materials are used in the construction of objects that are intended for use in sensitive and complex industries based on the two characteristics of low weight and high stiffness. In recent decades, these materials have been widely used in many industries. The use of composite beams in a variety of structures in disciplines such as mechanical engineering, nanotechnology, biomedical engineering, and aerospace engineering is well documented. Also, at the micro/nanoscale, the most notable examples of such applications include micro long spans, micro shafts, micro blades, nanowires, and microtubules [1]. In light of the profound practical significance of engineering, the present study is dedicated to investigating the vibration behavior of sandwich micro-beams. Porous materials are materials that have cavities or holes in their structure. The cellular structure of this category of porous materials is described by a network of gas-filled pores or voids in a matrix. In general, porosity factors minimize the overall weight of Functionally Graded (FG) porous structures. This material has many properties, such as being lightweight and good insulation. These materials are usually used as cores of sandwich structures due to their unique properties [2-7].

Some researchers have studied the vibration of microbeams with various reinforcements including carbon nanotubes (CNTs), carbon nanorods (CNRs), and graphene platelets (GPLs) [8-13]. Bargozini and Mohammadimehr [14] Discussed the behavior of nanocomposite beams reinforced with CNRs. They have employed both handmade and industrial methods to fabricate these composite sandwich beams. In their research, the synthesis of nanorods is achieved through a hydrothermal process, in which epoxy resin and CNRs derived from recycled materials are mixed together and subjected to a series of cycles to ensure uniform dispersion.

Arani et al. [15] employed free vibration and buckling sandwich microbeam and used MCST to capture the size effect for polymer piezoelectric nanocomposite face sheet, carbon nanotube fiber, with microactuator and microsensor on elastic foundation. Bamdad et al. [16] studied the vibration and buckling of a magneto-electroelastic sandwich Timoshenko beam. This beam has a porous core and a PVDF (polyvinylidene fluoride) layer whose properties depend on temperature. Based on the modified nonlocal elasticity theory, Rahmani et al. [17] illustrated the forced vibrations of a single-walled carbon nanotube under a moving harmonic load. Zenkour [18] investigated the thermal buckling analysis of carbon nanotubes in visco-Pasternak's medium. He investigated the

effects of foundation parameters, nonlocal parameters, and nanotube length on thermal buckling. In another work, Jena et al. [19-20] considered the buckling and vibration characteristics of nonlocal beams implanted in a Winkler-Pasternak elastic foundation. They used the von Kármán hypothesis to derive the governing equations of motion. Moreover, Bidgoli et al. [21] investigated the dynamic response and natural vibration characteristics of curved sandwich beams reinforced with porous cores, composite face sheets, and graphene platelets. The vibration and buckling of graphene platelets enhanced by porous beams were studied by Priyanka et al. [22], who exposed these platelets to different axial loads. Hosseini et al. [23] employed nonlocal strain gradient, material nonlinearity, and geometry to examine the nonlinear vibration of FG nanoporous beams. Ramteke et al. [24] investigated the impact of porosity on the mechanical and thermo-mechanical properties of FG materials. They employed a modeling approach to investigate the behavior of FG materials without explicitly delineating the solution methodologies employed.

Porous media are widely used in engineering structures due to their mechanical properties. In addition, carbon nanotubes or carbon nanorods have extraordinary physical properties that natural materials do not have. Furthermore, the size dependence effect becomes significant when the intrinsic length determined by the microstructure becomes comparable to the extrinsic length scale. That is to say, macrostructures have a size-dependence effect if the intrinsic length becomes comparable to its extrinsic length [25, 26] for the macroscale size effect. To consider the size effect at the micro-scale, some researchers [27, 28] have employed the size effect based on modified couple stress (MCST) or nonlocal strain gradient (NSGT) theories. Also, some physics bases have been recently developed for the nonlocal strain gradient theory [29]. Mohammadian [30] used a nonlocal strain gradient Timoshenko beam model to analyze the free vibrations of carbon nanotubes. The calibration of small-scale parameters was achieved by a combination of genetic algorithm and molecular dynamics simulations, demonstrating a multifaceted approach to scientific investigation. Eroğlu et al. [31]utilized the concept of high-order sinusoidal shear deformation concept to study the temperature-dependent characteristics of FG porous materials and the free vibration of the nanobeam. They also investigated the scale effects using NSGT. Nuhu et al. [32] recently reviewed new theories of elasticity, including micro and nanoplates for nonlinear bending.

They considered several classifications of documents when presenting these non-classical theories.

Some researchers worked on viscoelastic vibration analysis of a sandwich structure. Fatahi et al. [33] utilized a numerical model to forecast the performance of a piezoelectric energy harvester when situated on an auxetic substrate. They developed a numerical model to validate the performance of a piezoelectric beam. Mohammadi et al. [34] investigated the vibration behavior of a rotating viscoelastic nanobeam embedded in a visco-Pasternak foundation. The researchers investigated the influence of linear and nonlinear thermal stress cases, as well as humidity, on the vibrations of the viscoelastic nanobeam. Their findings revealed that the vibration frequencies in the nonlinear thermal stress case are smaller than those obtained in the linear thermal stress case. Safarabadi et al. [35] studied the free vibration behavior of rotating nanobeams, taking into account the surface effects on their vibration frequencies. Their findings indicated that softer boundary conditions resulted in an augmented influence of angular velocity on the nanobeam vibration frequencies.

Functionally graded materials for example, which have varying micro-structures from one material to another and the size of the microstructures involved ranges typically over several orders of magnitude, may not be adequately modeled by employing classical continuum mechanics alone but are probably more accurately analyzed using nonclassical continuum mechanics as well as using spatial variation of material properties. Li et al. [36] presented a free vibration analysis of nonlocal strain gradient beams made of functionally graded material. In their investigation of the nonlinear vibration characteristics of FG-GNPRC dielectric beams, Qian et al. [37] employed the Kelvin-Voigt model to capture the effects of internal damping. They derived the governing equations for the dielectric and viscoelastic Timoshenko beam by applying the effective medium theory and the rule of mixture to determine the material properties of the composites. Asgari et al. [38] investigated the simultaneous free vibration, buckling, and bending response of a sandwich beam with sinusoidal shear deformation theory for simply supported boundary conditions. In the study, they used a honeycomb core and shape memory alloy (SMA) in carbon nanotube-reinforced composite at the top and bottom of the core. The study showed with an enhancement in the thickness ratio, the heat flux decreases due to the increase in the thickness of the core. Brijeshgangil et al. [39] investigated the thermo-

mechanical properties of natural fiber-reinforced epoxy composites. Their study showed that the nanoparticles help in enhancing the interfacial bonding between the fiber and the composite. The study reported that nanoparticles exerted the most significant influence on the wear resistance of composites. Ni et al. [40] investigated the damped nonlinear dynamics of a cracked FG-GNPRC dielectric beam. Their analysis was based on Timoshenko's beam theory and von Kármán's nonlinear theory, which considers the effects of both mechanical excitation and electrical fields. They showed that the U, X, and O distributions have a minimal influence on the amplitude ratio. In another work, they [41] investigated the nonlinear vibration of FG-GNPRC dielectric beam with Kelvin-Voigt damping in a thermal environment. Jafari et al. [42, 43] worked on forced vibration control/active control of micro sandwich beams with various reinforced composites integrated by piezoelectric on Kerr's elastic foundation using MCST. Motalebi et al. [45] considered the vibration response of a sandwich plate reinforced by GPLs/GOAM.

A review of the extant literature indicates that the development of high-order porous FG microbeams and their mechanical properties with temperature dependence, considering the effect of thickness stretching, remains relatively unknown. In recent times, there has been a notable shift in focus among researchers towards the study of small-scale structures. It has been demonstrated that the classical theories that have hitherto been employed to examine the behavior of materials at a macro level are no longer capable of predicting the behavior of materials at a small scale. This has led to the identification of shortcomings in the application of micro and nano sizes within the classical theories. Consequently, a theoretical framework has been proposed for the investigation of material behavior at the micro and nano scales.

The present study is to investigate the vibration of a sandwich micro-beam using the shear and normal deformation beam theory (SNDBT) and the mechanical characteristics that depend on temperature, while, the previous research has delved into these topics individually. The integration of insights from previous research, the novelty of this study is to consider the free vibration analysis of a sandwich structure using shear and normal deformation beam theory (SNDBT) with a porous core and various reinforcing materials, including CNRs, GPLs, and CNTs by considering the size effect based on MCST/NSGT on various elastic foundations such as Winkler, Pasternak, and Kerr, simultaneously. It is also hypothesized that the mechanical properties of the face sheet layer

and porous core are dependent on temperature. Moreover, the thickness stretching effect and the incorporation of various porosity and functionally graded nanoparticle distributions on the natural frequency are investigated. On the other hand, this study contributes to practical engineering applications in a significant way.

2. Theory and Formulation

$$u(x,z,t)=u_0(x,t)-z\,\frac{\partial w_1(x,t)}{\partial x}+f(z)\frac{\partial w_2(x,t)}{\partial x} \quad (1)$$
$$w(x,z,t)=w_1(x,t)+w_2(x,t)+w_{st}(x,z,t)$$
$$v(x,z,t)=0$$

and

$$f(z)=\frac{-4z^3}{3h^2}$$
$$g(z)=(1-\frac{4z^2}{h^2})$$

In the displacement field, the axial displacement is considered as u_0, and the shear and bending components are defined as w_1, w_2. Also, w_{st} is the stretching effect and it is a function of z, x, and t that defined as:

$$w_{st}(x,z,t)=g(z)w_z(x,t) \quad (2)$$

where $w_z(x,t)$ denotes the normal displacement.

This study employs the shear and normal deformation theory to examine the analysis of a sandwich of higher-order micro-beams with porous cores and face sheets by considering reinforcements including carbon nanotubes (CNTs), carbon nanorods (CNRs) and graphene platelets (GPLs). The three-pattern core of a sandwich microbeam is composed of CNT reinforcements arranged in five functionally graded patterns that are varied in the thickness direction in the top and bottom face sheet.

A schematic representation of a sandwich beam is provided in Fig. 1a, which Fig. 1b illustrates the distribution of various types of carbon nanotubes (CNTs) throughout the face sheets and the porous core. The thickness of the face sheet layers is indicated by h_t and h_b, while the thickness of the core is indicated by h_c. In this model, it is assumed that there is a complete interconnection between the core and the face sheets. Figure 1.c illustrates the shape specification of the sandwich microbeam with a length of L, thicknesses of h_t, h_b for the top and bottom face layers, and also, h_c for a core thickness. The total thickness is $h=h_b+h_c+h_t$.

2.1. The Constitutive and Kinematics Equations

The displacement field of sandwich beams is determined by a higher-order normal and shear deformable beam, as expressed by the following equation. [22, 45, 46]:

The beam has a porous core and carbon nanotube-reinforced composite (CNTRC) on various elastic foundations including Kerr, Pasternak, and Winkler foundations as shown in Figures 1c,1d,1e, respectively.
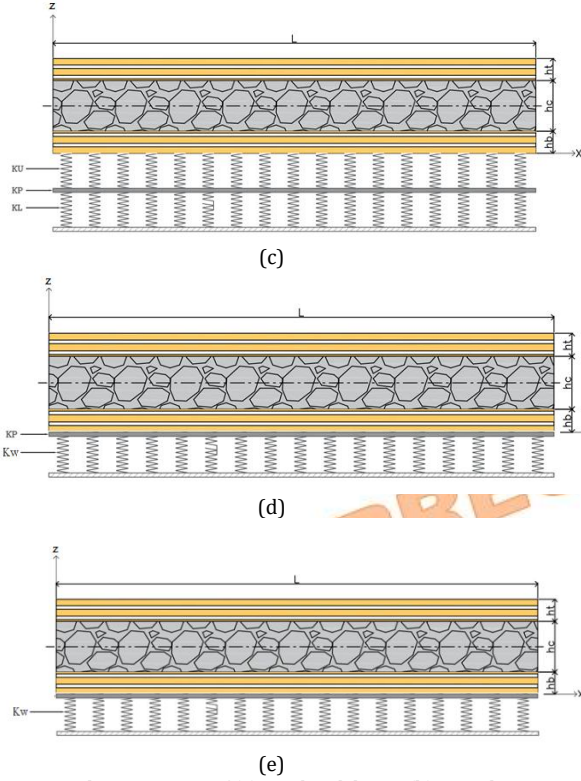

(a)

(b)

(c)

(d)

(e)
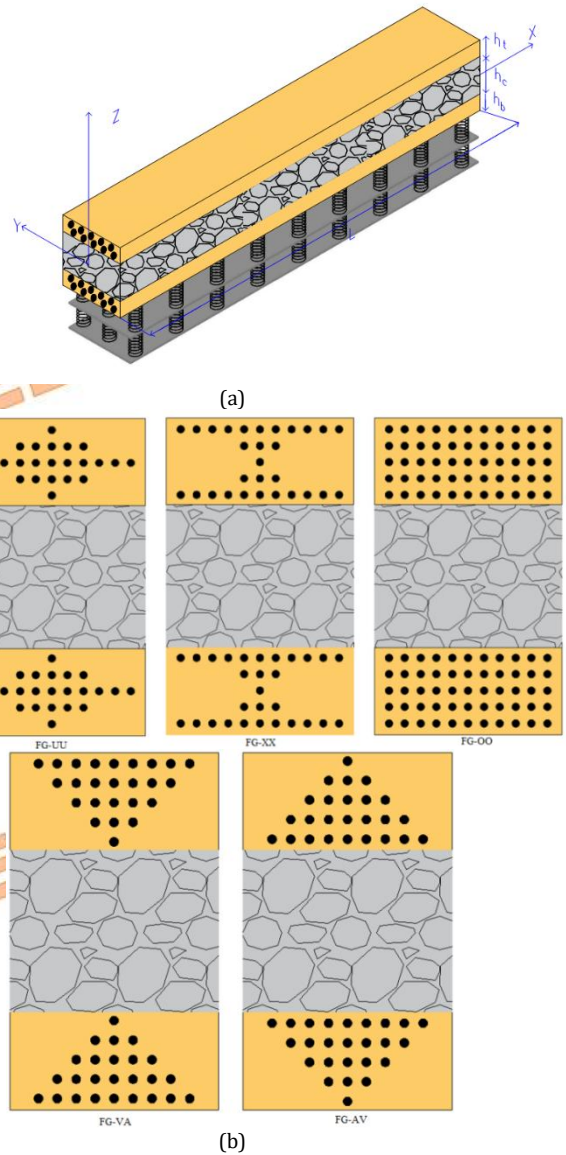
Fig. 1. A schematic view of (a) sandwich beam (b) Distribution with various types of CNTs in face sheets(c) A schematic view of porous core on Kerr's foundation(d) A schematic view of porous core on Pasternak's foundation (e) A schematic view of porous core on Winkler's foundation.

$$\varepsilon_x = \frac{\partial u}{\partial x} = \frac{\partial u_0}{\partial x} - z\frac{\partial^2 w_1}{\partial x^2} + f(z)\frac{\partial^2 w_2}{\partial x^2}$$

$$\varepsilon_z = \frac{\partial w}{\partial z} = \frac{-8z}{h^2}w_z(x,t) \tag{3}$$

$$\gamma_{xz} = \frac{\partial u}{\partial z} + \frac{\partial w}{\partial x} = g(z)(\frac{\partial w_2(x,t)}{\partial x} + \frac{\partial w_z(x,t)}{\partial x})$$

The assumption of core/skin (face sheet) is considered as follows:

1- It is assumed that the connection between the core and face sheet layers (skin) becomes as fully bonded. On the other hand, the delamination phenomenon does not occur.

2- In order to increase the strength-to-weight ratio in the structure, the weight of the core should be low, while the stiffness of the upper and lower face sheet layers (skin) should be high to increase this ratio.

The strain-displacement relations of the beam are obtained as follows:

where ε_x and ε_z are the normal strain in x and z directions, respectively. γ_{xz} is the shear strain.

The rotation about the x, y, and z axes can be prepared as follows:

$$\theta_x(x,z,t) = \frac{1}{2}(\frac{\partial w}{\partial y} - \frac{\partial v}{\partial z}) = 0$$

$$\theta_y(x,z,t) = \frac{1}{2}(\frac{\partial u}{\partial z} - \frac{\partial w}{\partial x}) = \frac{1}{2}(-\frac{\partial w_1}{\partial x} - \frac{4z^2}{h^2}\frac{\partial w_2}{\partial x} - \frac{\partial w_1}{\partial x} - \frac{\partial w_2}{\partial x} - (1-\frac{4z^2}{h^2})\frac{\partial w_z}{\partial x}) \tag{4}$$

$$\theta_z(x,z,t) = \frac{1}{2}(\frac{\partial v}{\partial x} - \frac{\partial u}{\partial y}) = 0$$

where $\theta_i(i=x,y,z)$ are the rotation of the x, y, and z axes based on the modified couple stress theory.

The constitutive equations for the face sheets and core are defined as follows:

$$\sigma_{ij}^{f,c} = Q_{ijkl}\varepsilon_{kl} \tag{5}$$

in which stress and strain components of a sandwich micro-beam are illustrated by σ_{ij} and ε_{kl}, respectively. For each layer, Q_{ijkl} denotes the stiffness matrix components.

The linear constitutive equations for the bottom and top face sheet layers are presented as follows:

$$\sigma^{t,b}_{xx} = Q_{11}\varepsilon_{xx} + Q_{13}\varepsilon_{zz}$$

$$\sigma^{t,b}_{zz} = Q_{31}\varepsilon_{xx} + Q_{33}\varepsilon_{zz} \tag{6}$$

$$\sigma^{t,b}_{xz} = Q_{55}\gamma_{xz}$$

where Q_{11}, Q_{22}, Q_{55}, Q_{13} and Q_{33} are the elastic stiffness for the top and bottom face sheet layers.

In addition, the constitutive equations of the core are expressed as follows:

$$\sigma^c_{xx} = Q_{11}\varepsilon_{xx} + Q_{13}\varepsilon_{zz}$$

$$\sigma^c_{zz} = Q_{31}\varepsilon_{xx} + Q_{33}\varepsilon_{zz} \tag{7}$$

$$\sigma^c_{xz} = Q_{55}\gamma_{xz}$$

where:

5

$$Q_{11} = Q_{22} = \frac{E(z)}{1-v^2}$$

$$Q_{55} = \frac{E(z)}{2(1+v)} \qquad (8)$$

$$Q_{13} = Q_{31} = \frac{E(z)v}{1-v^2}$$

2.2. The Size Effects at Micro Scale

The size-dependent mechanical behavior has been observed experimentally, thus, the size effect should be taken into account for structures at the micro-scale. However, the non-classical continuum theories established to facilitate small-scale composites, such as the strain gradient elasticity, nonlocal theory, the couples stress theory, the modified couple stress theory, and the nonlocal strain gradient theory, are employed to conduct studies concentrated on vibration behavior response. Dynamic analysis of these structures at the micro-scale is performed using small-scale theories. At the nanoscale, nonlocal theory is employed. In their previous articles, the authors have compared these theories and concluded that the NSGT theory has yielded superior results at the micro-scale, thus in the present study, the nonlocal strain gradient theory is considered for a sandwich beam.

2.2.1. Nonlocal Strain Gradient Theory

The nonlocal strain gradient theory (NSGT) has recently been considered a prominent model for elucidating the structural mechanics at the micro-scale. This theory explicitly incorporates the nonlocal and material length scale parameters. By integrating nonlocal and strain gradient effects into traditional continuum mechanics, NSGT enables a more comprehensive understanding at the micro-scale. Numerous studies have adopted NSGT to investigate the mechanical behavior of these structures [47]. At the micro-scale, intermolecular forces and size-dependent effects become significant, and

classical continuum mechanics is unable to analyze the behavior of structures at this scale. Consequently, a series of size-dependent continuous medium mechanics theories have been presented by scientists. The nonlocal theory encompasses the micro-force information between atoms and molecules. This theory has been extensively applied in the domain of nano-mechanics [48-49]. The elastic materials are defined by the fact that the state of stress is determined by the strains at all other body locations through the use of NSGT. [50-51]. In the nonlocal theory, the components of the mechanical stress tensor at an arbitrary spot are dependent on the strain components at all spots. This assumption is consistent with intramolecular interactions between distinct locations at the nanoscale. [50-51].

$$\left[1 - \mu \nabla^2\right]\sigma_{ij} = C_{ijkl}\left[1 - l_0^2\nabla^2\right]\varepsilon_{kl} \qquad (9)$$

where $\mu = (ea)^2$ and l_0 are nonlocal and strain gradient parameters, respectively.

2.2.2. Modified Couple Stress Theory

The modified couple stress theory is considered the size effect at the micro-scale. The curvature equation, strain energy variation, and kinematic energy variation of this theory, which is dependent on the small size effect, are expressed as follows. [45]:

$$m_{ij} = 2(l_m)^2 \mu(z)\chi_{ij} \qquad (10)$$

where l_m, χ_{ij} are material length scale parameters, and curvature tensor and $\mu(z) = Q_{44}$ is Lame's parameter.

By employing the rotation vector in Eq. (4), the following result is obtained:

$$\chi_{yz} = \frac{1}{2}\left(\frac{\partial \theta_y}{\partial z} + \frac{\partial \theta_z}{\partial y}\right) = \frac{1}{4}\left(\frac{-8z}{h^2}\frac{\partial w_2}{\partial x} + \frac{8z}{h^2}\frac{\partial w_z}{\partial x}\right)$$

$$\chi_{xy} = \frac{1}{2}\left(\frac{\partial \theta_x}{\partial y} + \frac{\partial \theta_y}{\partial x}\right) = \frac{1}{4}\left(-2\frac{\partial^2 w_1}{\partial x^2} - \frac{4z^2}{h^2}\frac{\partial^2 w_2}{\partial x^2} - \frac{\partial^2 w_2}{\partial x^2} - \left(1 - \frac{4z^2}{h^2}\right)\frac{\partial^2 w_z}{\partial x^2}\right) \qquad (11)$$

$$\chi_{xx} = \chi_{yy} = \chi_{xz} = \chi_{zz} = 0$$

2.3. The Materials Properties for Face Sheets and Core

Carbon nanotubes were discovered by [52] rolling graphene platelets. Based on the reaction parameters of the synthesis route employed, a variety of CNTs can be produced.

In this article, the rule of mixture is required to determine the effective properties of materials. Consequently, the effects of elastic and shear modulus for nanocomposite materials are correlated.

The mechanical properties of the face sheet are considered for PMMA material to be strengthened with single-walled carbon

6

nanotubes following the equation as the extended mixture rule. [11, 16, 53, 54]:

$$E_{11} = \eta_1 E_{11CNT} V_{CNT} + V_m E_m,$$

$$\frac{\eta_3}{G_{12}} = \frac{V_{CNT}}{G_{12CNT}} + \frac{V_m}{G_m},$$

$$\rho_f = V_{CNT}\rho_{CNT} + V_m\rho_m, \quad (12)$$

$$\upsilon_f = V_{CNT}\upsilon_{CNT} + V_m\upsilon_m,$$

$$V_{CNT} + V_m = 1$$

where E_{11CNT} and E_m denote the value of Young's modulus of CNTs and matrix for nanocomposite, respectively, G_{12CNT} and G_m are the shear modulus of CNTs and matrix, respectively, ρ_{CNT}, ρ_m are the density of CNTs and matrix and V_{CNT} and V_m are the volume fractions of the CNTs and matrix, respectively.

According to the CNT distribution patterns, the volume fraction of CNTs (V_{CNT}) is defined as follows

$FG:V$

$$VCNT_t^b = \left(1 + \frac{2}{h_b^t}\left(z \pm \frac{h_c + h_t^b}{2}\right)\right)V_{CNT}$$

$FG:A$

$$VCNT_t^b = \left(1 - \frac{2}{h_b^t}\left(z \pm \frac{h_c + h_t^b}{2}\right)\right)V_{CNT}$$

$FG:X$

$$VCNT_t^b = \frac{4|z|}{h_t^b}V_{CNT} \quad (13)$$

$FG:O$

$$VCNT_t^b = 2\left(1 - \frac{2}{h_b^t}\left(z \pm \frac{h_c + h_t^b}{2}\right)\right)V_{CNT}$$

In this research, the influence of the material face sheet and the material core are considered to be temperature dependent. The specification of the face sheets and the core of the three-layer micro-beam are expected to vary based on temperature. The influence of the top and bottom surface layers of the material is investigated and compared with CNR and GPL. There are variations in CNT dispersion across the thickness of these sandwich beam face sheet layers. In this sandwich beam model, the aligned CNTs are symmetrical on the top and bottom face sheet layers.

Table 1. The mechanical properties of matrix and CNTs for temperature-dependent materials [55]

Material	properties	
CNT	$E_{11CNT}(Pa)$	$((1 + (1.5849 \times 10^4) \times (\Delta T) + (3.5390 \times 10^7) \times (\Delta T)^2 + (-3.7070 \times 10^{-10}) \times (\Delta T)^3)) \times (5.6466 \times 10^{12})$
	$G_{12CNT}(Pa)$	$((1 + (8.3093 \times 10^5) \times (\Delta T) + (-1.7803 \times 10^7) \times (\Delta T)^2 + (8.5651 \times 10^{-11}) \times (\Delta T)^3)) \times (1944.5 \times 10^9)$
	$\alpha(1/{}^0K)$	$((1 + (2.5039 \times 10^3) \times (\Delta T) + (-5.3839 \times 10^6) \times (\Delta T)^2 + (3.2738 \times 10^{-11}) \times (\Delta T)^3)) \times (3.4584 \times 10^9)$
	$\rho_{CNT}(kg/m^3)$	1400
	υ_{CNT}	0.175
Matrix	$E_m(Pa)$	$(3.52 - 0.0034 \times T)10^9$

Table 2. The mechanical properties of CNR for temperature-dependent materials [14]

Material	properties	
CNR	$E_{11CNR}(Pa)$	$(0.76798 - 0.00052061 \times T + 0.0000008916 \times T^2 - 0.535 \times 10^9 \times T^3) \times 10^{12}$
	$G_{12CNR}(Pa)$	$(0.16891 + 0.000417145 \times T - 0.0000005358 \times T^2 + 0.5375 \times 10^9 \times T^3) \times 10^{12}$
	$\alpha(1/{}^0K)$	$(-0.13502 + 0.00275003 \times T - 0.0000034644 \times T^2 + 0.1364 \times 10^8 \times T^3) \times 10^{-6}$
	$\rho_{CNR}(kg/m^3)$	1400

υ_{CNR}	0.175

The intermediate layer of this beam model is made of porous material, and Fig. 1 depicts the geometry of a porous core with dimensions of length. L and thickness h_c. Also, $E(z), G(z), \rho(z)$ are Young's modulus, shear modulus, and density of porous core, respectively that are defined for various porous core distributions as follows [55, 57, 58]:

Symmetric distribution

Table 3. The mechanical properties of GPL with temperature-dependent materials [56]

Material	Properties	
GPL	$E_{11GPL}(Pa)$	$(1087.8 - 0.261T) \times 10^9$
	$\alpha(1/{}^0K)$	$(13.92 - 0.0299T) \times 10^{(-6)}$
	$\rho_{GPL}(kg/m^3)$	1062.5
	υ_{GPL}	0.186

$$E(z) = E_1(1 - e_0 \cos(\frac{\pi z}{h}))$$
$$G(z) = G_1(1 - e_0 \cos(\frac{\pi z}{h}))$$
$$\rho(z) = \rho_1(1 - e_m \cos(\frac{\pi z}{h_c})) \qquad (14)$$

Asymmetric distribution

$$E(z) = E_1(1 - e_0 \cos(\frac{\pi z}{h} + \frac{\pi}{4}))$$
$$G(z) = G_1(1 - e_0 \cos(\frac{\pi z}{h} + \frac{\pi}{4})) \qquad (15)$$
$$\rho(z) = \rho_1(1 - e_m \cos(\frac{\pi z}{h_c} + \frac{\pi}{4}))$$

Uniform distribution

$$E(z) = E_1(1 - e_0 \psi)$$
$$G(z) = G_1(1 - e_0 \psi) \qquad (16)$$
$$\rho(z) = \rho_1(1 - e_0 \sqrt{1 - e_0 \psi})$$

$$\psi = \frac{1}{e_0} - \frac{1}{e_0}(\frac{2}{\pi}\sqrt{1 - e_0} - \frac{2}{\pi} + 1)^2 \qquad (17)$$

Where e_0 and e_m are the porosity parameters that are defined as follows:

$$e_0 = 1 - \frac{E_1}{E_2}$$
$$\qquad (18)$$
$$e_m = 1 - \frac{\rho_1}{\rho_2}$$

The equation of thermoelasticity proposed by Toloukian and Ho is considered as follows.[31, 56].

$$P = P_0 * (P_{(-1)} T^{(-1)} + P_1 T + P_2 T^2 + P_3 T^3 + 1) \qquad (19)$$

The temperature-dependent material constants of the porous core, which is composed of SUS304, Si3O4, and ZrO2 are considered in Table 4 [57, 60].

Table 4. Mechanical properties of the porous core with temperature-dependent material constants

Material	properties	$P_{(-1)}$	P_0	P_1	P_2	P_3
SUS304	$E(Pa)$	0	201.01×10^9	3.079×10^{-4}	-6.534×10^{-7}	0
	$\alpha(1/{}^0K)$	0	12.33×10^{-6}	8.086×10^{-4}	0	0
	$\rho(kg/m^3)$	0	8166	0	0	0
	υ	0	0.3262	-2.002×10^{-4}	3.797×10^{-7}	0
ZrO2	$E(Pa)$	0	244.27×10^9	-1.371×10^{-3}	1.214×10^{-6}	-3.681×10^{-10}
	$\alpha(1/{}^0K)$	0	12.766×10^{-6}	-1.491×10^{-3}	1.006×10^{-5}	-6.778×10^{-11}
	$\rho(kg/m^3)$	0	3657	0	0	0
	υ	0	0.2882	1.133×10^{-4}	0	0

Si3O4	$E(Pa)$	0	348.43×10^{9}	-3.070×10^{-4}	2.160×10^{-7}	-8.946×10^{-11}
	$\alpha(1/{}^{0}K)$	0	5.8723×10^{-6}	9.095×10^{-4}	0	0
	$\rho(kg/m^{3})$	0	2370	0	0	0
	υ	0	0.24	0	0	0

2.4. The Governing Equations of Motion

The equations of motion are obtained by Hamilton's principle as follows:

$$\int_{0}^{t}\delta\Pi dt=\int_{0}^{t}(\delta T-\delta U)dt=0 \tag{20}$$

where δT represents the variation of the kinetic energy, while δU denotes the variation of the strain energy. Consequently, the initial step is to ascertain the strain energy of the sandwich microbeam, which encompasses both the face sheets and the core.

The strain energy variation can be written based on MCST as follows:

$$\delta U=\int\int_{-\frac{h_c}{2}-h_t}^{\frac{h_c}{2}+h_t}\sigma_{xx}(\delta\varepsilon_x)+\sigma_{zz}(\delta\varepsilon_z)+\sigma_{xz}(\delta\gamma_{xz})+m_{xy}\delta(\chi_{xy})+m_{yz}\delta(\chi_{yz})dzdA \tag{21}$$

The sandwich micro beams are placed on an elastic foundation, in which, Kerr's model elastic foundation consists of k_S shear layer stiffness, k_u and k_l are the upper and lower spring stiffness, δU_f is reported as follows:

$$\delta U_f=\int\delta U_{Kerr}dA=\int f_e^{Kerr}\delta wdA$$

$$f_e^{\ker r}=(\frac{k_lk_u}{k_l+k_u})w-(\frac{k_Sk_u}{k_l+k_u})\nabla^2w$$

$$=(\frac{k_lk_u}{k_l+k_u})(w_1(x,t)+w_2(x,t)+g(z)w_z(x,t))-(\frac{k_Sk_u}{k_l+k_u})\nabla^2(w_1(x,t)+w_2(x,t)+g(z)w_z(x,t))$$

$$\tag{22}$$

where k_S is the shear layer stiffness, k_u and k_l are the upper and lower spring stiffness.

The Pasternak's and Winkler's foundation models are defined as follows:

Pasternak's,

$$\delta U_f=\int\delta U_{Pasternak}dA=\int f_e^{Pasternak}\delta wdA$$

$$f_e^{Pasternak}=(k_w)w-(k_p)\nabla^2w$$

$$=(k_w)(w_1(x,t)+w_2(x,t)+g(z)w_z(x,t))-(k_p)\nabla^2(w_1(x,t)+w_2(x,t)+g(z)w_z(x,t)) \tag{23}$$

where k_w and k_p are two parameters of elastic foundations.

Winkler's,

$$\delta U_f=\int\delta U_{Winkler}dA=\int f_e^{Winkler}\delta wdA$$

$$f_e^{Winkler}=(k_w)w$$

$$=(k_w)(w_1(x,t)+w_2(x,t)+g(z)w_z(x,t)) \tag{24}$$

where k_w is the spring constant of the Winkler foundation.

Then, the variations of the kinetic energy for the sandwich micro-beam are obtained as follows:

$$\delta T=\int\int_{-\frac{h_c}{2}-h_t}^{\frac{h_c}{2}+h_t}\rho\frac{\partial u}{\partial t}(\delta\frac{\partial u}{\partial t})dz+\rho\frac{\partial w}{\partial t}\delta(\frac{\partial w}{\partial t})dzdA \tag{25}$$

The governing equations of motion for a sandwich micro-beam can be derived by

9

considering the strain energy, kinetic energy, and nonlocal constitutive relations using NSGT. Substituting Eq. (17) into Eqs. (20) and (22), the

corresponding relationships are obtained as follows:

$$\delta u_0 : (1 - l_0^2\nabla^2)\left(\frac{\partial N_x}{\partial x}\right) = \left(1 - (ea)^2\nabla^2\right)\left(I_0\frac{\partial^2 u_0}{\partial t^2} - I_1\frac{\partial^3 w_1}{\partial x\partial t^2}\right)$$

$$\delta w_1 : (1 - l_0^2\nabla^2)\left(\frac{\partial^2 M_x}{\partial x^2} + \frac{1}{2}\frac{\partial^2 M_{xy}^{(0)}}{\partial x^2}\right) - (1 - (ea)^2\nabla^2)f_e^{\ker r} = \left(1 - (ea)^2\nabla^2\right)(I_1\frac{\partial^3 u_0}{\partial x\partial t^2} - I_2\frac{\partial^4 w_1}{\partial x^2\partial t^2} + I_{fz}\frac{\partial^4 w_2}{\partial x^2\partial t^2}$$
$$+ I_0\frac{\partial^2 w_1}{\partial t^2} + I_0\frac{\partial^2 w_2}{\partial t^2} + I_g\frac{\partial^2 w_z}{\partial t^2})$$

$$\delta w_2 : (1 - l_0^2\nabla^2)\left(\frac{4}{3h^2}\frac{\partial^2 f_{xx}}{\partial x^2} - \frac{4}{h^2}\frac{\partial g_x}{\partial x} + \frac{\partial Q_X}{\partial x} + \frac{1}{h^2}\frac{\partial^2 M_{xy}^{(2)}}{\partial x^2} + \frac{1}{4}\frac{\partial^2 M_{xy}^{(0)}}{\partial x^2} - \frac{2}{h^2}\frac{\partial M_{yz}^{(1)}}{\partial x}\right) - (1 - (ea)^2\nabla^2)f_e^{\ker r} = \qquad (26)$$
$$\left(1 - (ea)^2\nabla^2\right)(-I_f\frac{\partial^3 u_0}{\partial x\partial t^2} + I_{fz}\frac{\partial^4 w_1}{\partial x^2\partial t^2} - I_{ff}\frac{\partial^4 w_2}{\partial x^2\partial t^2} + I_0\frac{\partial^2 w_1}{\partial t^2} + I_0\frac{\partial^2 w_2}{\partial t^2} + I_g\frac{\partial^2 w_z}{\partial t^2})$$

$$\delta w_z : (1 - l_0^2\nabla^2)\left(\frac{8}{h^2}M_z + \frac{\partial Q_X}{\partial x} - \frac{4}{h^2}\frac{\partial g_x}{\partial x} + \frac{1}{4}\frac{\partial^2 M_{xy}^{(0)}}{\partial x^2} - \frac{1}{h^2}\frac{\partial^2 M_{xy}^{(2)}}{\partial x^2} + \frac{2}{h^2}\frac{\partial M_{yz}^{(1)}}{\partial x}\right) - (1 - (ea)^2\nabla^2)g(z)f_e^{\ker r}$$
$$= \left(1 - (ea)^2\nabla^2\right)(I_g\frac{\partial^2 w_1}{\partial t^2} + I_g\frac{\partial^2 w_2}{\partial t^2} + I_{gg}\frac{\partial^2 w_z}{\partial t^2})$$

where the resultant forces and moments in Eq. (26) are defined in Appendix A. By substituting Eq. (3), (6), and (7) into Eqs. Appendix A, the

governing equations of motion for a sandwich beam are obtained as follows:

$$\delta u_0 :$$

$$A^{(0)}\frac{\partial^2 u_0}{\partial x^2} - A^{(1)}\frac{\partial^3 w_1}{\partial x^3} - \frac{4A^{(3)}}{3h^2}\frac{\partial^3 w_2}{\partial x^3} - \frac{8B^{(1)}}{h^2}\frac{\partial w_z}{\partial x} - l_0^2(A^{(0)}\frac{\partial^4 u_0}{\partial x^4} - A^{(1)}\frac{\partial^5 w_1}{\partial x^5} - \frac{4A^{(3)}}{3h^2}\frac{\partial^5 w_2}{\partial x^5} \qquad (27)$$
$$- \frac{8B^{(1)}}{h^2}\frac{\partial^3 w_z}{\partial x^3}) = (1 - (ea)^2\nabla^2)(I_0\frac{\partial^2 u_0}{\partial t^2} - I_1\frac{\partial^3 w_1}{\partial x\partial t^2} + I_f\frac{\partial^3 w_2}{\partial x\partial t^2})$$

$$\delta w_1 :$$

$$A^{(1)}\frac{\partial^3 u_0}{\partial x^3} - A^{(2)}\frac{\partial^4 w_1}{\partial x^4} - \frac{4A^{(4)}}{3h^2}\frac{\partial^4 w_2}{\partial x^4} - \frac{8B^{(2)}}{h^2}\frac{\partial^2 w_z}{\partial x^2} - l_0^2(A^{(1)}\frac{\partial^5 u_0}{\partial x^5} - A^{(2)}\frac{\partial^6 w_1}{\partial x^6} - \frac{4A^{(4)}}{3h^2}\frac{\partial^6 w_2}{\partial x^6}$$
$$- \frac{8B^{(2)}}{h^2}\frac{\partial^4 w_z}{\partial x^4}) - \frac{C^{(0)}}{2}\frac{\partial^4 w_1}{\partial x^4} - \frac{C^{(2)}}{h^2}\frac{\partial^4 w_2}{\partial x^4} - \frac{C^{(0)}}{4}\frac{\partial^4 w_2}{\partial x^4} - \frac{C^{(0)}}{4}\frac{\partial^4 w_z}{\partial x^4} + \frac{C^{(2)}}{h^2}\frac{\partial^4 w_z}{\partial x^4} - l_0^2(-\frac{C^{(0)}}{2}\frac{\partial^6 w_1}{\partial x^6} \qquad (28)$$
$$- \frac{C^{(2)}}{h^2}\frac{\partial^6 w_2}{\partial x^6} - \frac{C^{(0)}}{4}\frac{\partial^6 w_2}{\partial x^6} - \frac{C^{(0)}}{4}\frac{\partial^6 w_z}{\partial x^6} + \frac{C^{(2)}}{h^2}\frac{\partial^6 w_z}{\partial x^6} - (1 - (ea)^2\frac{\partial^2}{\partial x^2})f_e^{\ker r} = (1 - (ea)^2\nabla^2)(I_1\frac{\partial^3 u_0}{\partial x\partial t^2} - I_2\frac{\partial^4 w_1}{\partial x^2\partial t^2}$$
$$+ I_{fz}\frac{\partial^4 w_2}{\partial x^2\partial t^2} + I_0\frac{\partial^2 w_1}{\partial t^2} + I_0\frac{\partial^2 w_2}{\partial t^2} + I_g\frac{\partial^2 w_z}{\partial t^2})$$

10

δw_2:

$$\frac{4A^{(3)}}{3h^2}\frac{\partial^3 u_0}{\partial x^3} - \frac{4A^{(4)}}{3h^2}\frac{\partial^4 w_1}{\partial x^4} - \frac{16A^{(6)}}{9h^4}\frac{\partial^4 w_2}{\partial x^4} - \frac{32B^{(4)}}{3h^4}\frac{\partial^2 w_z}{\partial x^2} - I_0^2\left(\frac{4A^{(3)}}{3h^2}\frac{\partial^5 u_0}{\partial x^5} - \frac{4A^{(4)}}{3h^2}\frac{\partial^6 w_1}{\partial x^6} - \frac{16A^{(6)}}{9h^4}\frac{\partial^6 w_2}{\partial x^6}\right.$$
$$\left. - \frac{32B^{(4)}}{3h^4}\frac{\partial^4 w_z}{\partial x^4}\right) + \frac{16E^{(4)}}{h^4}\frac{\partial^2 w_2}{\partial x^2} - \frac{4E^{(2)}}{h^2}\frac{\partial^2 w_2}{\partial x^2} - 4E^{(2)}\frac{\partial^2 w_z}{\partial x^2} + \frac{16E^{(4)}}{h^4}\frac{\partial^2 w_z}{\partial x^2} - I_0^2\left(\frac{16E^{(4)}}{h^4}\frac{\partial^4 w_2}{\partial x^4}\right.$$
$$- \frac{4E^{(2)}}{h^2}\frac{\partial^4 w_2}{\partial x^4} - \frac{4E^{(2)}}{h^2}\frac{\partial^4 w_z}{\partial x^4} + \frac{16E^{(4)}}{h^4}\frac{\partial^4 w_z}{\partial x^4} - \frac{4E^{(2)}}{h^2}\frac{\partial^2 w_z}{\partial x^2} + E^{(0)}\frac{\partial^2 w_2}{\partial x^2} + E^{(0)}\frac{\partial^2 w_z}{\partial x^2} - \frac{4E^{(2)}}{h^2}\frac{\partial^2 w_z}{\partial x^2}\right)$$
$$- I_0^2\left(-\frac{4E^{(2)}}{h^2}\frac{\partial^4 w_2}{\partial x^4} + E^{(0)}\frac{\partial^4 w_2}{\partial x^4} + E^{(0)}\frac{\partial^4 w_z}{\partial x^4} - \frac{4E^{(2)}}{h^2}\frac{\partial^4 w_z}{\partial x^4}\right) - C^{(2)}\frac{\partial^4 w_1}{\partial x^4} - 2C^{(4)}\frac{\partial^4 w_2}{\partial x^4} - \frac{C^{(2)}}{h^2}\frac{\partial^4 w_2}{\partial x^4}$$
$$+ \frac{2C^{(4)}}{h^4}\frac{\partial^4 w_z}{\partial x^4} - \frac{C^{(2)}}{h^4}\frac{\partial^4 w_z}{\partial x^4} - I_0^2\left(-\frac{C^{(2)}}{h^2}\frac{\partial^6 w_1}{\partial x^6} - \frac{2C^{(4)}}{h^2}\frac{\partial^6 w_2}{\partial x^6} - \frac{C^{(2)}}{h^4}\frac{\partial^6 w_2}{\partial x^6} + \frac{2C^{(4)}}{h^4}\frac{\partial^6 w_z}{\partial x^6} - \frac{C^{(2)}}{h^4}\frac{\partial^6 w_z}{\partial x^6}\right)$$
$$- \frac{C^{(0)}}{4}\frac{\partial^4 w_1}{\partial x^4} - \frac{C^{(2)}}{2h^2}\frac{\partial^4 w_2}{\partial x^4} - \frac{C^{(0)}}{8}\frac{\partial^4 w_z}{\partial x^4} - I_0^2\left(-\frac{C^{(0)}}{4}\frac{\partial^6 w_1}{\partial x^6} - \frac{C^{(2)}}{2h^2}\frac{\partial^6 w_2}{\partial x^6}\right.$$
$$\left. - \frac{C^{(0)}}{8}\frac{\partial^6 w_2}{\partial x^6} - \frac{C^{(0)}}{8}\frac{\partial^6 w_z}{\partial x^6} + \frac{C^{(2)}}{2h^2}\frac{\partial^6 w_z}{\partial x^6}\right) + \frac{8}{h^2}C^{(2)}\frac{\partial^2 w_2}{\partial x^2} - \frac{8}{h^4}C^{(2)}\frac{\partial^2 w_z}{\partial x^2} - I_0^2\left(\frac{8}{h^2}C^{(2)}\frac{\partial^4 w_2}{\partial x^4} - \frac{8}{h^2}C^{(2)}\frac{\partial^4 w_z}{\partial x^4}\right)$$
$$- \left(1 - (ea)^2\frac{\partial^2}{\partial x^2}\right)f_e^{\mathrm{ker}\,r} = \left(1 - (ea)^2\nabla^2\right)\left(-I_f\frac{\partial^3 u_0}{\partial x\partial t^2} + I_{fz}\frac{\partial^4 w_1}{\partial x^2\partial t^2} - I_{ff}\frac{\partial^4 w_2}{\partial x^2\partial t^2} + I_0\frac{\partial^2 w_1}{\partial t^2} + I_0\frac{\partial^2 w_2}{\partial t^2} + I_g\frac{\partial^2 w_z}{\partial t^2}\right) \tag{29}$$

δw_z:

$$\frac{8}{h^2}B^{(1)}\frac{\partial u_0}{\partial x} - 8\frac{B^{(2)}}{h^2}\frac{\partial^2 w_1}{\partial x^2} - \frac{32B^{(4)}}{3h^4}\frac{\partial^2 w_2}{\partial x^2} - \frac{64F^{(2)}}{h^4}w_z - I_0^2\left(\frac{8}{h^2}B^{(1)}\frac{\partial^3 u_0}{\partial x^3} - 8\frac{B^{(2)}}{h^2}\frac{\partial^4 w_1}{\partial x^4}\right.$$
$$\left. - \frac{32B^{(4)}}{3h^4}\frac{\partial^4 w_2}{\partial x^4} - \frac{64F^{(2)}}{h^4}\frac{\partial^2 w_z}{\partial x^2}\right) - \frac{4E^{(2)}}{h^2}\frac{\partial^2 w_2}{\partial x^2} + E^{(0)}\frac{\partial^2 w_2}{\partial x^2} + E^{(0)}\frac{\partial^2 w_z}{\partial x^2} - \frac{4E^{(2)}}{h^2}\frac{\partial^2 w_z}{\partial x^2}$$
$$- I_0^2\left(-\frac{4E^{(2)}}{h^2}\frac{\partial^4 w_2}{\partial x^4} + E^{(0)}\frac{\partial^4 w_2}{\partial x^4} + E^{(0)}\frac{\partial^4 w_z}{\partial x^4} - \frac{4E^{(2)}}{h^2}\frac{\partial^4 w_z}{\partial x^4}\right) + \frac{16E^{(4)}}{h^4}\frac{\partial^2 w_2}{\partial x^2} - \frac{4E^{(2)}}{h^2}\frac{\partial^2 w_z}{\partial x^2}$$
$$- \frac{4E^{(2)}}{h^2}\frac{\partial^2 w_z}{\partial x^2} + \frac{16E^{(4)}}{h^4}\frac{\partial^2 w_z}{\partial x^2} - I_0^2\left(\frac{16E^{(4)}}{h^4}\frac{\partial^4 w_2}{\partial x^4} - \frac{4E^{(2)}}{h^2}\frac{\partial^4 w_z}{\partial x^4} - \frac{4E^{(2)}}{h^2}\frac{\partial^4 w_z}{\partial x^4} + \frac{16E^{(4)}}{h^4}\frac{\partial^4 w_z}{\partial x^4}\right)$$
$$+ \left(\frac{-C^{(0)}}{4}\frac{\partial^4 w_1}{\partial x^4} - \frac{C^{(2)}}{2h^2}\frac{\partial^4 w_2}{\partial x^4} - \frac{C^{(0)}}{8}\frac{\partial^4 w_2}{\partial x^4} - \frac{C^{(0)}}{8}\frac{\partial^4 w_z}{\partial x^4} + \frac{C^{(2)}}{2h^2}\frac{\partial^4 w_z}{\partial x^4} - I_0^2\left(\frac{-C^{(0)}}{4}\frac{\partial^6 w_1}{\partial x^6} - \frac{C^{(2)}}{2h^2}\frac{\partial^6 w_2}{\partial x^6}\right.\right.$$
$$\left.\left. - \frac{C^{(0)}}{8}\frac{\partial^6 w_2}{\partial x^6} - \frac{C^{(0)}}{8}\frac{\partial^6 w_z}{\partial x^6} + \frac{C^{(2)}}{2h^2}\frac{\partial^6 w_z}{\partial x^6}\right)\right) + \left(\frac{C^{(2)}}{2h^2}\frac{\partial^4 w_1}{\partial x^4} + \frac{2C^{(4)}}{h^4}\frac{\partial^4 w_2}{\partial x^4} - \frac{C^{(2)}}{2h^2}\frac{\partial^4 w_z}{\partial x^4} + \frac{2C^{(4)}}{h^4}\frac{\partial^4 w_z}{\partial x^4}\right.$$
$$\left. - \frac{8}{h^2}C^{(2)}\frac{\partial^4 w_2}{\partial x^4} - I_0^2\left(+\frac{C^{(2)}}{2h^2}\frac{\partial^6 w_1}{\partial x^6} + \frac{2C^{(4)}}{h^4}\frac{\partial^6 w_2}{\partial x^6} + \frac{C^{(2)}}{2h^2}\frac{\partial^4 w_z}{\partial x^4} - \frac{2C^{(4)}}{h^4}\frac{\partial^6 w_z}{\partial x^6} + \frac{2h^2}{C^{(2)}}\frac{\partial^6 w_2}{\partial x^6}\right)\right) - \frac{8C^{(2)}}{h^4}\frac{\partial^2 w_2}{\partial x^2}$$
$$+ \frac{8C^{(2)}}{h^4}\frac{\partial^2 w_z}{\partial x^2} - I_0^2\left(-\frac{8C^{(2)}}{h^4}\frac{\partial^4 w_2}{\partial x^4} + \frac{8C^{(2)}}{h^4}\frac{\partial^4 w_z}{\partial x^4}\right)$$
$$- \left(1 - (ea)^2\frac{\partial^2}{\partial x^2}\right)g(z)f_e^{\mathrm{ker}\,r} = \left(1 - (ea)^2\frac{\partial^2}{\partial x^2}\right)\left(I_g\frac{\partial^2 w_1}{\partial t^2} + I_g\frac{\partial^2 w_2}{\partial t^2} + I_{gg}\frac{\partial^2 w_z}{\partial t^2}\right) \tag{30}$$

where the variables in Eqs. (27)-(30) are defined in Appendix B.

3. Solution Procedure

In order to obtain solutions to the governing equations of motion for a sandwich micro-beam, it is possible to employ an analytical procedure based on Navier's technique. In the present study, this analytical procedure is used to identify solutions to the aforementioned equations, which are formulated as follows [61]:

$$\begin{Bmatrix} u_0(x,t) \\ w_1(x,t) \\ w_2(x,t) \\ w_z(x,t) \end{Bmatrix} = \sum_{m=1}^{\infty} \begin{Bmatrix} U_m \cos(\frac{m\pi}{L}x)e^{i\omega_m t} \\ W_{1m}\sin(\frac{m\pi}{L}x)e^{i\omega_m t} \\ W_{2m}\sin(\frac{m\pi}{L}x)e^{i\omega_m t} \\ W_{zm}\sin(\frac{m\pi}{L}x)e^{i\omega_m t} \end{Bmatrix} \tag{31}$$

By substituting Eqs. (31) into Eqs. (27)-(30), the stiffness and mass matrices have obtained that are shown in Appendix C,D.

4. Validation Study

The initial step in the process is to verify the accuracy of the current work's outcomes. This may be accomplished by comparing the outcome of straightforward examples with an analysis of earlier research. This section includes an analytical assessment of the vibration behavior in a microcomposite beam including three layers.

First, the proposed methodology is validated by comparing the findings with the most recent research in this field. Comparison of dimensionless natural frequencies of simply supported micro symmetric ($\theta/-\theta/\theta$) composite beams whose material properties are assumed to

11

be $E_1 = 144GPa,\ E_2 = E_3 = 9.65GPa,$

$G_{23} = 3.45GPa,\ G_{12} = G_{13} = 4.14GPa$

$,\upsilon_{12} = \upsilon_{13} = \upsilon_{23} = 0.3,\ h = 25\mu m,$

$\rho = 1389.23\dfrac{kg}{m^3},\dfrac{L}{h} = 5$

Table 5 presents a comparison of the dimensionless natural frequencies resulting from this solution, along with the corresponding results [22].

Table 5. Comparison of the dimensionless natural frequencies micro composite beam between present work and obtained results by [22]

	Ref. [22]	Present work
Theory	Shear and normal beam theory	Shear and normal beam theory
Solution method	Ritz Solution Method	Naveir's solution
Orientation (θ)		
0	1.8501	1.8508
15	1.3396	1.4968
30	0.9232	0.8321
45	0.7533	0.7494
60	0.6968	0.6905
75	0.6914	0.6867
90	0.6960	0.6900

5. Results and Discussion

5.1. Parametric Study

This study uses, CNT, GPL and CNR face sheet materials as reinforcement (see Tables 1, 2, and 3). SUS304, Si$_3$N$_4$, and ZrO$_2$ are used as the porous core. Table 4 shows the material properties of the core. The sandwich beam has a length of $L = 880\mu m$, a thickness of top and bottom face sheet layers becomes $h_t = 8.8\mu m$ and $h_b = 8.8\mu m$, respectively, and a core thickness of $h_c = 158.4\mu m$. The following values are used for analysis: following values are considered for analytical evaluation, efficiency parameter of CNTs, $\eta_1 = 0.137, \eta_2 = 1.022, \eta_3 = 0.715$, coefficients of porosity $e_0 = 0.6$, volume fractions of CNTs and matrix PMMA $V_{CNT} = 0.12, V_m = 0.88$. It is considered nonlocal

parameter $(ea)^2 = 2\mu m$, the strain gradient parameter $l_0 = 17.6\mu m$ and the modified couple stress parameter $l_m = 17.6\mu m$.

5.2. Vibration Analysis

The results for vibration analysis of a sandwich micro beam according to the normal and shear deformation theory are obtained. The relationships and mechanical properties for a sandwich porous beam with CNTs/CNRs/GPLs face sheets, whose are presented in Tables 1,2,3.

As shown Figure 2, comparing the frequency of the non-local strain gradient with various thickness ratios, increasing the thickness of the core causes to decrease the natural frequency because the stiffness of the micro-sandwich beam reduces. This figure shows how the thickness of a sandwich micro beam changes compared to its total thickness. On the other hands, when the h_c/h thickness ratio increases, the stiffness of the micro beam decreases. In addition, it shows in this figure that for $L/l_0 = 75, h_c = 0.9h$ is compared to $h_c = 0.5h$, as the microbeam becomes thinner, the stiffness decreases. As a result, the natural frequency decreases by 55%.
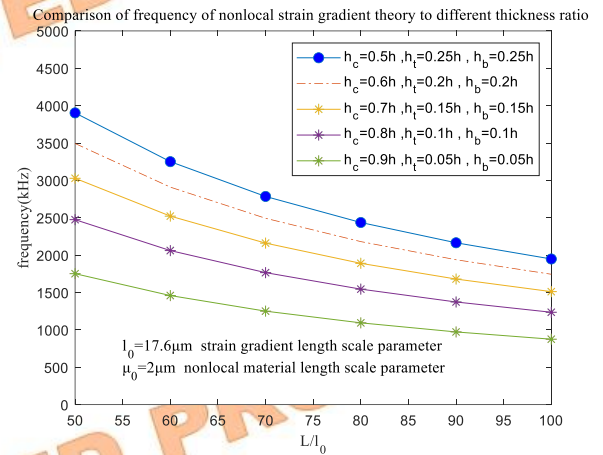
Fig. 2. The effect of thickness ratio on the natural frequency

This study considers both types of continuum theories, namely nonlocal and strain gradient parameters. The impact of varying l_0 and $\mu = (ea)^2$ on the frequency is also demonstrated in Figs. 3a and 3b, respectively. It can be observed that as the length-to-thickness ratio increases, the frequency declines. Additionally, when different strain gradient parameters are used, the results show that the natural frequency increases. In addition, it shows in Fig. 3a that for $L/h = 5$, $l_0 = 17.6\mu m$ compared to $l_0 = 10\mu m$, when the strain gradient parameter get smaller, the stiffness gets lower. This causes the natural frequency to decrease by 43%. The findings

indicate that the implementation of the nonlocal strain gradient theory enables the stiffening of the sandwich microbeam as the strain gradient parameter increases.

Figures 3b and 3c illustrate the impact of the nonlocal parameter on the natural frequency of a sandwich microbeam, with $l_0 = 17.6 \mu m, V_{CNT} = 0.12, \Delta T = 25^0 K$. As illustrated in the figure, an increase in slenderness ratio results in a reduction in frequency. Additionally, the figures show a noticeable decrease in the slope of the curve as the nonlocal parameter increases. This phenomenon is attributed to the significant influence of the nonlocal parameter on the stiffness of the structure. The aforementioned phenomena indicate that the utilization of the nonlocal parameter enables the sandwich microbeam to manifest softening behaviors, with the increase of this parameter. In addition, in this Fig. 3c shows that for $L/h = 5$, $(ea)^2 = 4 \mu m$ compared to $(ea)^2 = 12 \mu m$, An increase in the nonlocal parameter is associated with a decrease in stiffness. This causes the natural frequency to decrease by 66.5%. The significance of the small-scale parameter in the mechanical analysis of microstructures has been demonstrated.

Furthermore, it is shown from the figures that the influence of small length scale parameters on the frequency is significant. It is shown that by increasing the strain gradient parameter and the nonlocal parameter, the natural frequency increases and decreases, respectively.
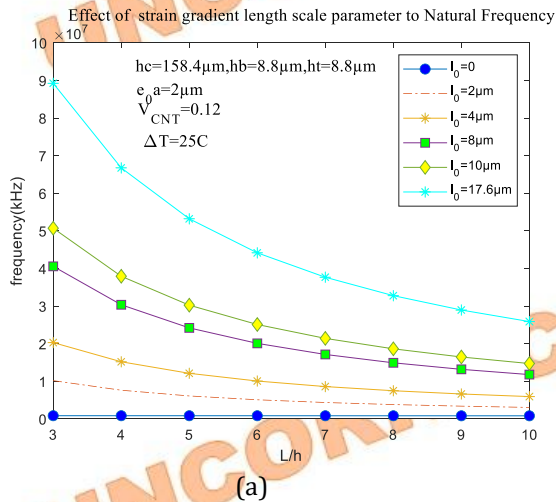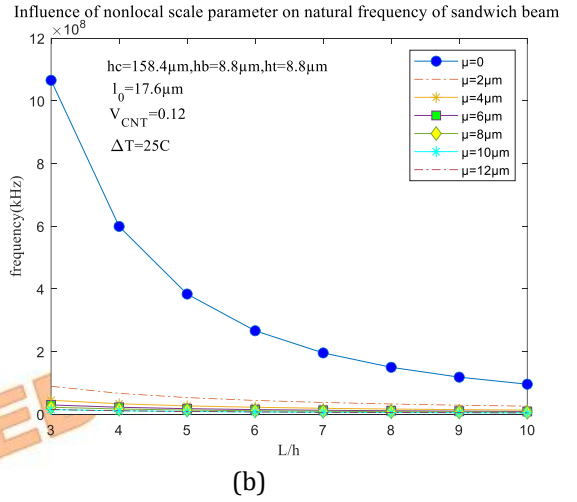
(b)
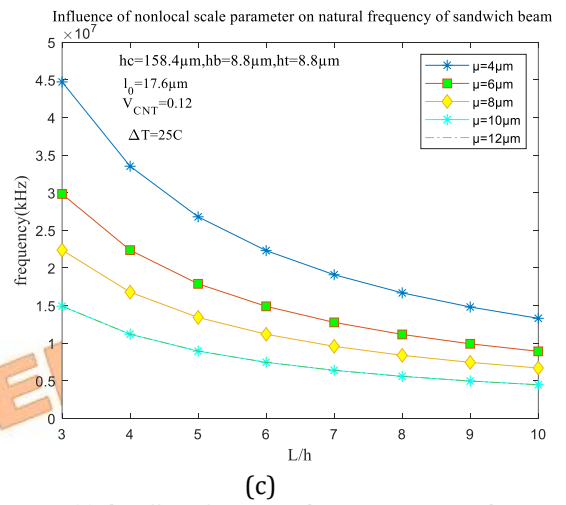
(c)

Fig. 3. (a) the effect of strain gradient parameter on the natural frequency, (b, c) the effects of nonlocal parameter on the natural frequency

Figure 4 illustrates the vibration of a sandwich microbeam for the nonlocal parameter. The effect of different nonlocal parameters on first four natural frequencies are considered. It is shown that by increasing this parameter, the low and high frequencies of the microbeams decrease. These results indicate that the nonlocal parameters of the beam exert a greater influence on the high frequencies of sandwich microbeams than on the low frequencies. Calibration the nonlocal parameter and strain gradient parameters is attributed to the significant influence of the nonlocal parameter on the stiffness of the structure. Using Figs. 3 and 4, one can obtain the calibration of the nonlocal parameter and strain gradient parameters.
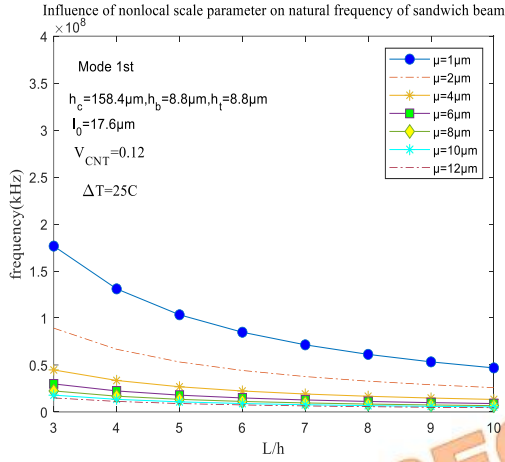
(a)

Influence of nonlocal scale parameter on natural frequency of sandwich beam

(a)

Influence of nonlocal scale parameter on natural frequency of sandwich beam

(b)

Influence of nonlocal scale parameter on natural frequency of sandwich beam

(c)

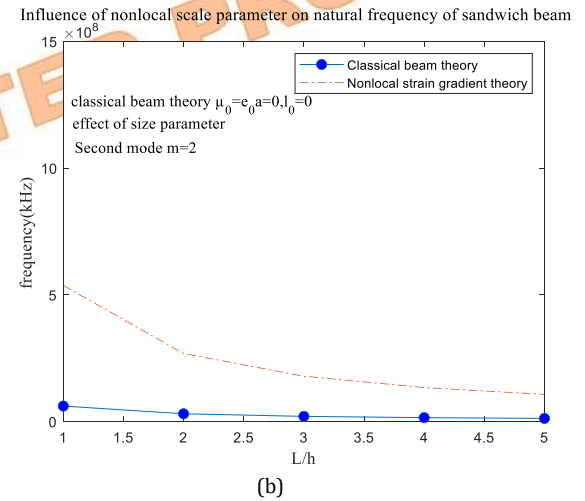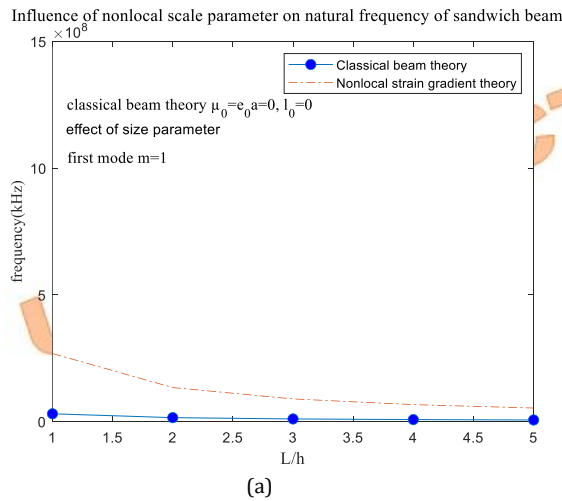Influence of nonlocal scale parameter on natural frequency of sandwich beam

(d)
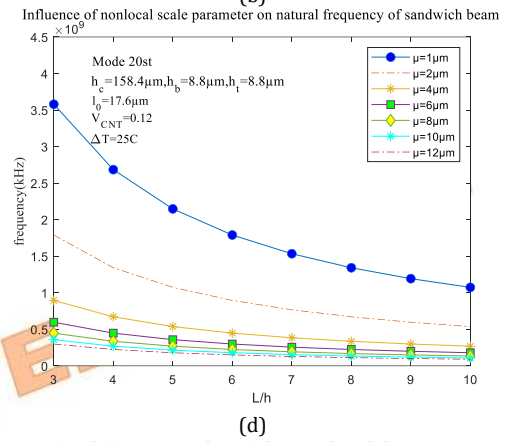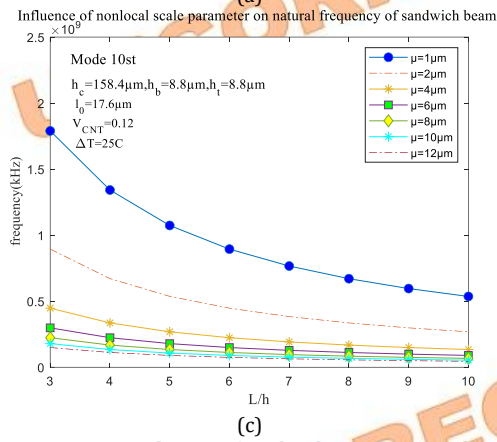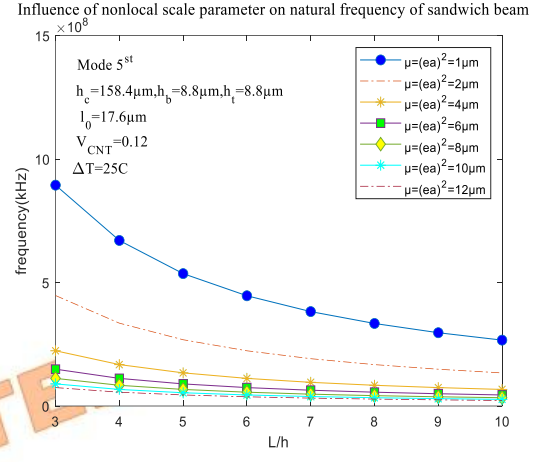
Fig. 4. Influence of nonlocal parameter on the natural frequency for different modes of the sandwich beam

As stated by NSGT, two size effect parameters, namely, the nonlocal parameter $\mu = (ea)^2$ and the strain gradient parameter l_0 are considered on the vibration behavior of the sandwich microbeam. As illustrated in Fig. 5, the impact of the size parameter on the first four natural frequencies of the sandwich microbeam is plotted against L/h. As illustrated in the figure, the frequency of NSGT rises when both the nonlocal parameter and the strain gradient parameter are taken into account. The application of this model results in a stiffening behavior for the sandwich microbeam, in comparison to the classical theory. Thus, this result leads to an increase in the value of frequency.

Influence of nonlocal scale parameter on natural frequency of sandwich beam

(a)

Influence of nonlocal scale parameter on natural frequency of sandwich beam

(b)

14

(c)

(d)
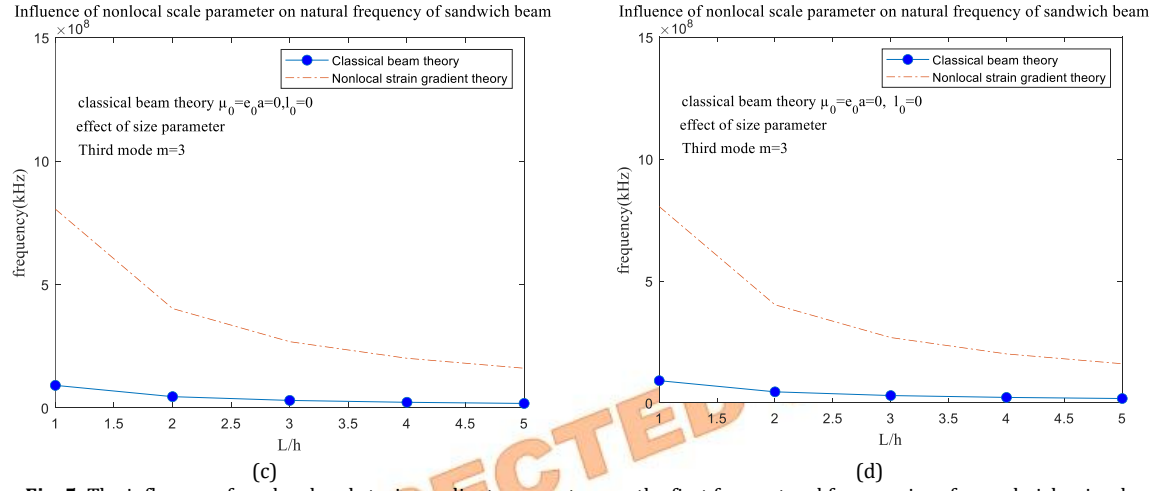
Fig. 5. The influence of nonlocal and strain gradient parameters on the first four natural frequencies of a sandwich microbeam

The stretching parameter (w_{st}) in the displacement field is employed to account for the variation along the thickness direction. Figures 6a b illustrate the impact of the thickness stretching effect on the natural frequency of a sandwich microbeam. It can be observed that the frequency of sandwich beams is overestimated for $L/h > 7$, indicating that thee thickness stretching effect has been overlooked. The results demonstrate that the SNDBT theory is capable of accounting for the thickness stretching effect and accurately predicting the frequency for varying length-to-thickness ratios.

(a)

Effect of thickness stretching to Natural Frequency

(b)
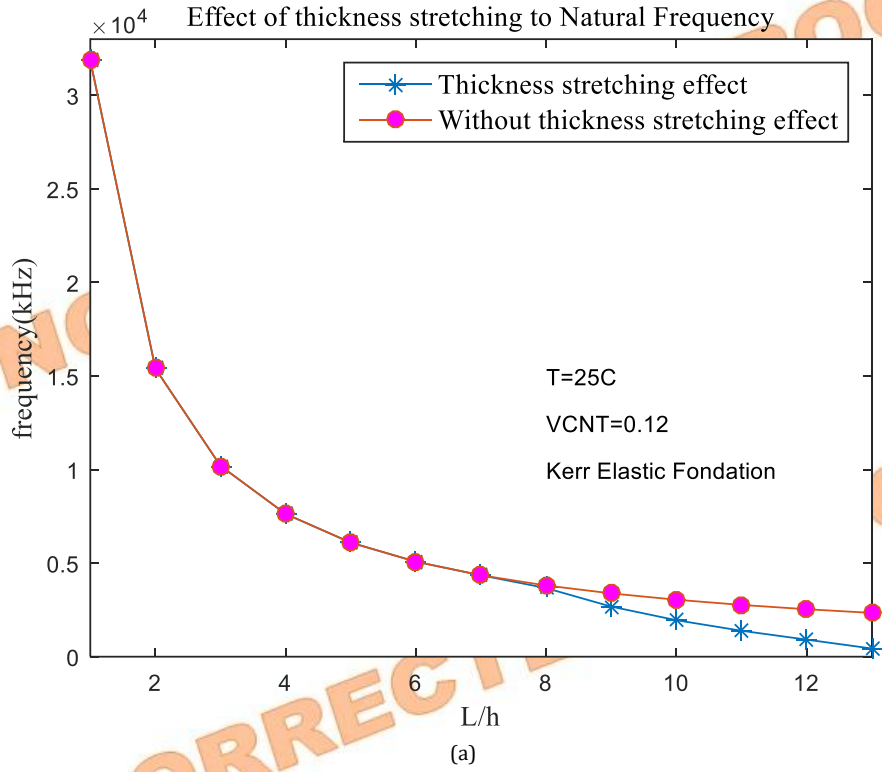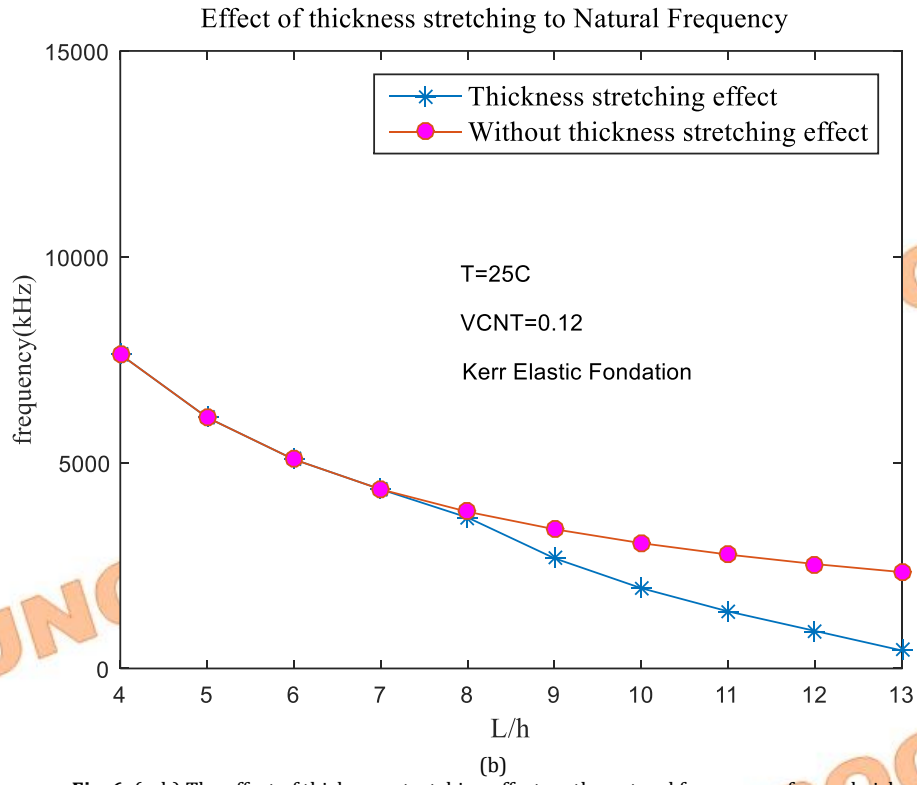
Fig. 6. (a, b) The effect of thickness stretching effect on the natural frequency of a sandwich microbeam

Figure 7 illustrates the influence of aspect ratio on frequency for varying volume fractions of CNTs. Aspect ratio (L/h) has been observed to result in a decline in the natural frequency, as evidenced in Fig. 7. It is shown that with increasing the volume fractions of CNTs, the stiffness of a sandwich microbeam increases and also, it leads to enhance the natural frequency.
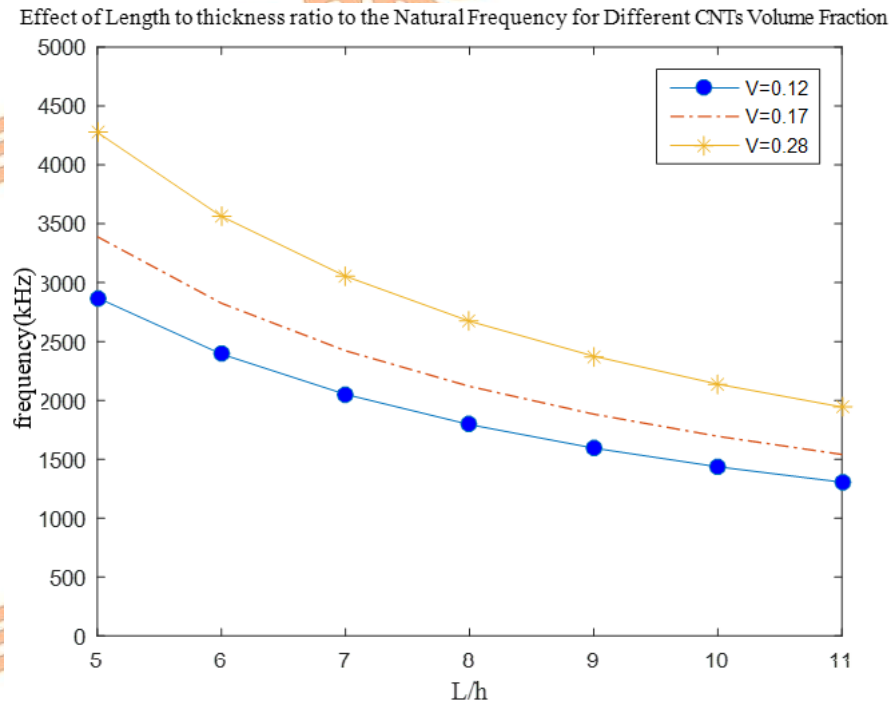
Fig. 7. Length Influence to microbeam thickness ratio for different CNTs volume fraction on the natural frequency

Figure 8a shows the effect of various distributions of carbon nanotubes (CNTs) including FG-AV, FG-XX, FG-UU, FG-OO and FG-VA on the natural frequency. The results demonstrate that the FG-OO distribution exhibits

the lowest natural frequency, while the FG-XX distribution has the opposite effect. Additionally, the beam's inherent frequency reaches its maximum when the FG-XX CNT distribution is applied. The structural stiffness and natural frequency of the structure change when different reinforcement distributions are used in the face sheet layer. The natural frequency increases by 67.4%, when FG-XX is compared to FG-UU face sheets, and it decreases by 24.8% when FG-OO is compared to FG-UU. Fig. 8b illustrates the impact of the porosity coefficient on the natural frequency of the sandwich beams. This figure depicts how the frequency of the beams decreases as the porosity coefficient of the core

increases. In the experimental results, one can be mixed the resin with carbon nanotubes or carbon nanorods by ultrasonic tools. In this case, it is assumed that two materials (matrix as well as nano particles) are mixed as uniform, (one can see [13], and [14]) while; in practice, it is not possible as functionally graded that they mixed. Then, the created nanocomposite is placed upper and lower porous core layers. In theoretical results, the functionally graded carbon nanotubes using Eq. (13) for the top and bottom face sheets in a sandwich structure are considered. Figure 8 shows the various natural frequency distributions.

Effect of length to thickness of the beam to Natural Frequency for various distributions
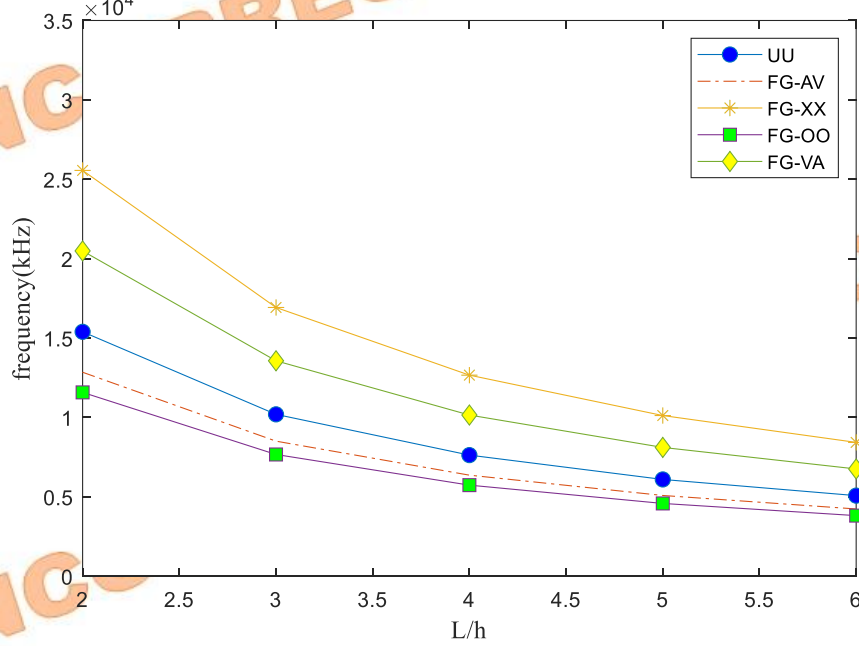
(a)

Effects of the porosity coefficient Core (e_0) on the natural frequency

(b)

17
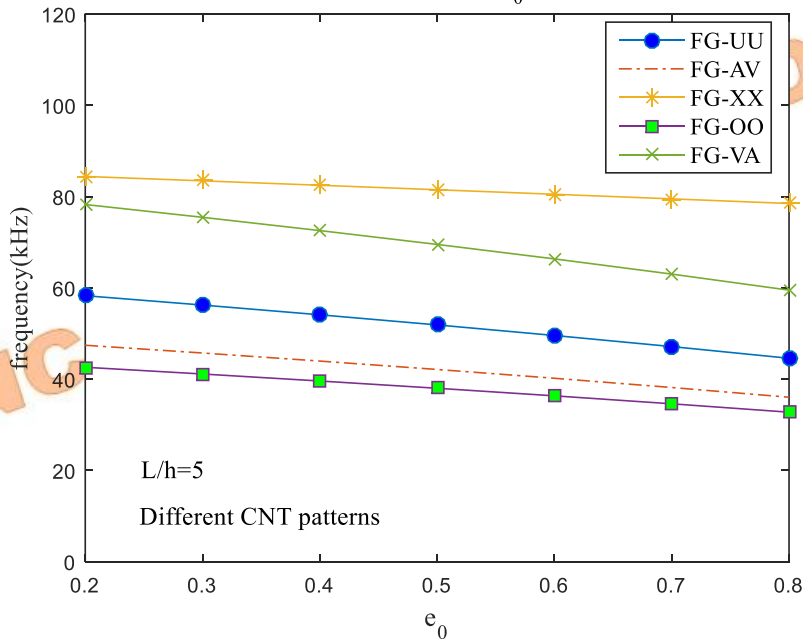
Fig. 8. (a) The influence of aspect ratio on natural frequency for different CNTs distribution, (b) Porosity coefficient effects (e_0) core
on the natural frequency for different CNT patterns

Figure 9 illustrates the influence of the core-to-face sheet thickness ratio (h_c / h_f) on frequency. on frequency. As the beam's aspect ratio increases,

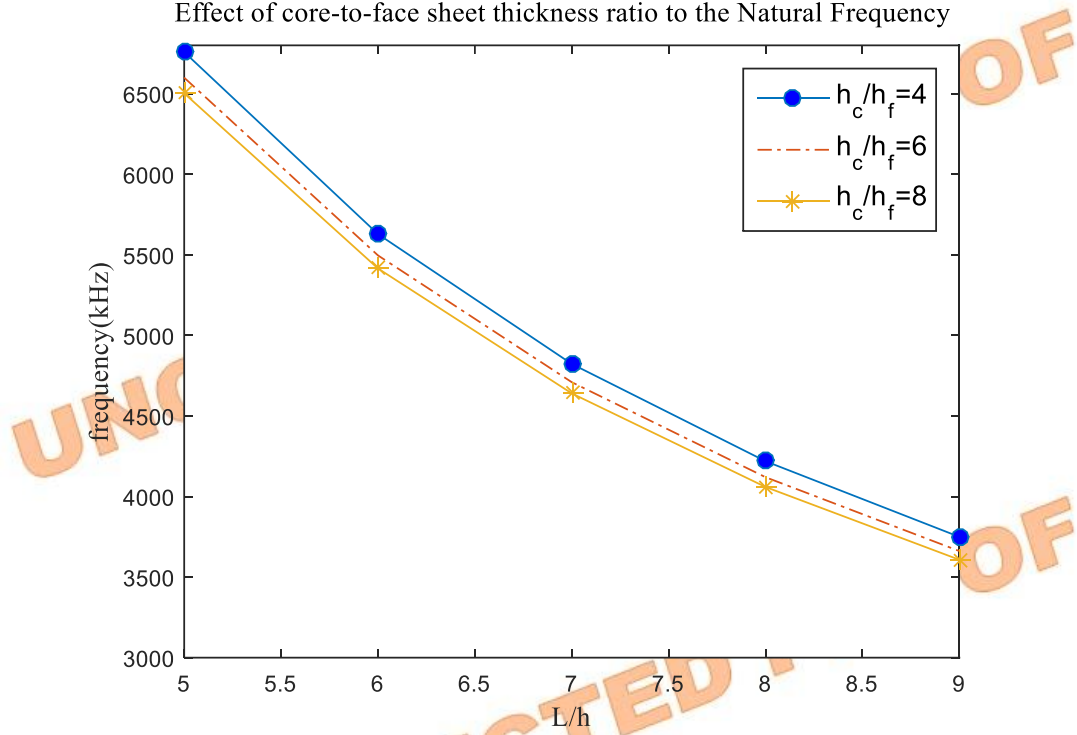the frequency decreases. An increase in the ratio of h_c / h_f results in a reduction in the values of natural frequency, indicating a softer structure.

Effect of core-to-face sheet thickness ratio to the Natural Frequency

Fig. 9. Influence of core-to-face sheet thickness ratio of a sandwich microbeam to natural frequency

The influence of various porosity distributions including asymmetric, symmetric, and uniform distributions on the natural frequency is illustrated in Fig. 10. The natural frequency values are highest in

asymmetric distributions and lowest in uniform distributions.

Effect of thicknesses ratio to frequency for Different porosity distribution
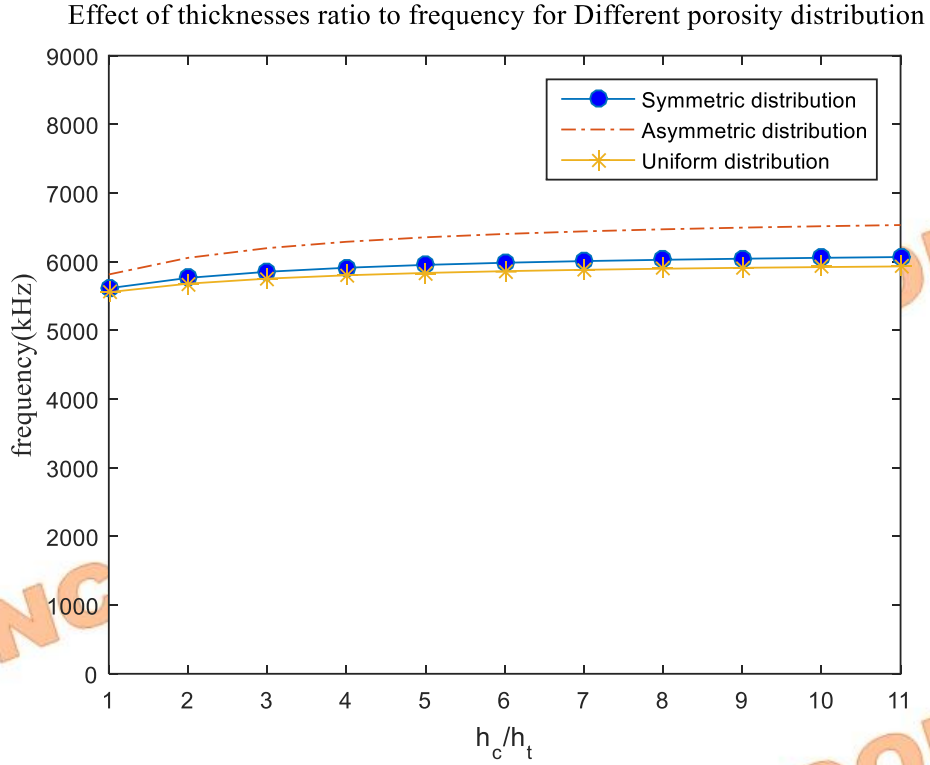
Fig. 10. Influence of thicknesses ratio for different porosity distribution types on the natural frequency

Figure 11 shows how the frequency of a sandwich beam is affected by the various types of reinforcement including (CNT, CNR, GPL) in the face sheet layer. As the figure shows, graphene platelets (GPL) have the highest frequency, followed by carbon nano rods (CNRs), which have the lowest frequency. To verify and compare the nanomaterials used in this study, it has been shown that adding reinforcement increases the frequency of beams with $\frac{L}{h} = 5$. The sandwich beams are compared to without reinforcement, by an increase in the volume fraction of the reinforcements, the stiffness and the frequency of the sandwich micro beam increases. The GPLs increase the frequency by 10%, the CNTs by 7%, and the CNRs by 4%. It has been shown that adding reinforcement has been demonstrated to enhance both the stiffness and the frequency of the sandwich beam. CNRs are used as reinforcement that are made with cheap materials. They are similar to another nanocomposite in terms of mechanical properties. CNRs are much more economical than CNTs because they are made using a green process [14]. This makes them a good alternative for nanocomposites in many industries.
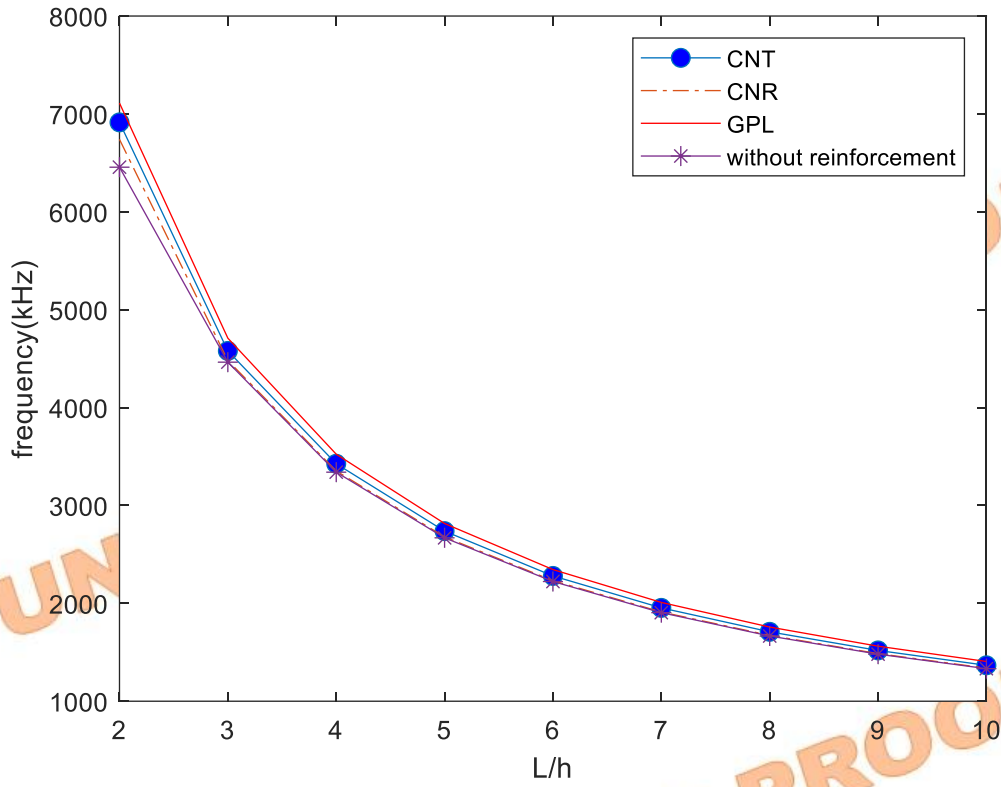
Fig. 11. The effect of various reinforcements in the face sheet layers on natural frequency of a sandwich microbeam

Figure 12a illustrates the frequency behavior of the microbeam for three distinct elastic foundations: Winkler's, Pasternak's and Kerr's foundations. It can be observed that an increase in frequency is evident when considering the stiffness of the aforementioned foundations. As illustrated in Figure 12b, the consideration of Kerr elastic foundation compared to without any elastic foundation increases the natural frequency of a sandwich microbeam.

Effect of different elastic foundation on natural frequency

(a)

Effect of different elastic foundation on natural frequency

(b)
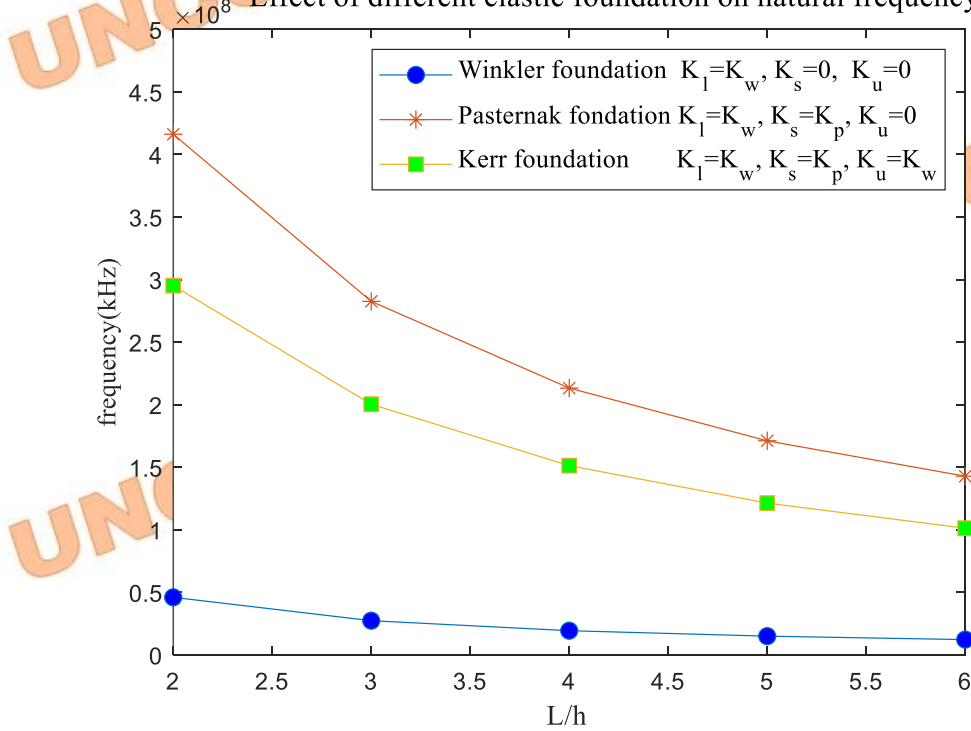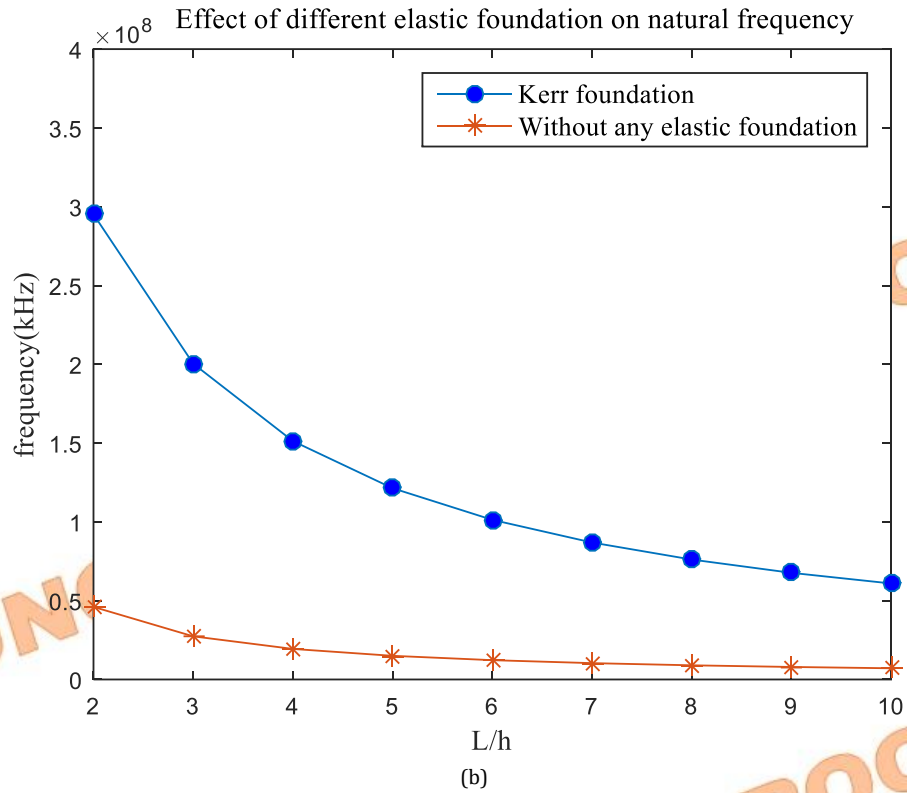
Fig. 12. (a, b) Effect of different elastic foundation on natural frequency

Figure 13a illustrates the effect of different Kerr elastic foundation parameters on the natural frequency. It can be observed from this figure that an increase in shear layer stiffness K_s parameter leads to enhance in the natural frequency. Figure 13b shows the variation of the upper elastic foundation on the natural frequency. It can be concluded that an increase in the elastic foundation parameters results in an increase in the frequency of the structure. Furthermore, it is evident that the stiffness of the springs (K_u, K_l) plays a significant role in the vibrational behavior of the system.

Effect of shear layer stiffness(K_s) on natural frequency for different thickness ratio L/h

(a)

21
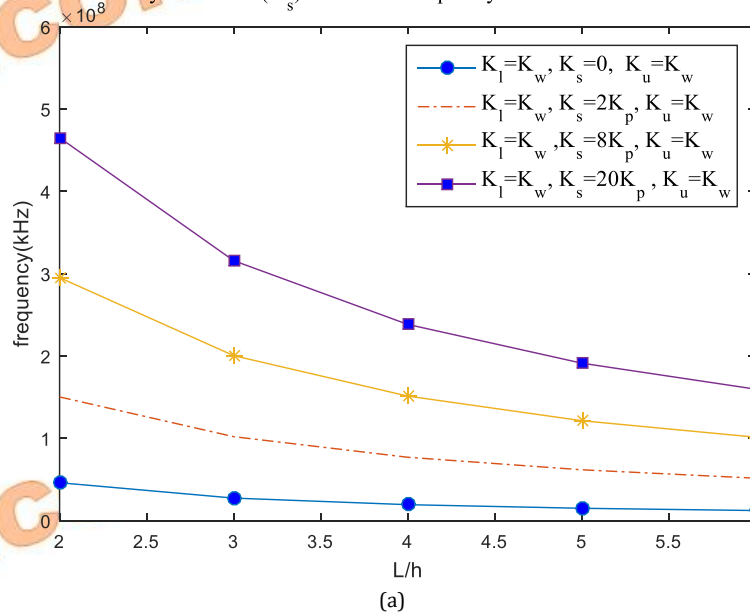
Effect of different Kerr elastic foundation parameters (K_l, K_s, K_u) on natural frequency
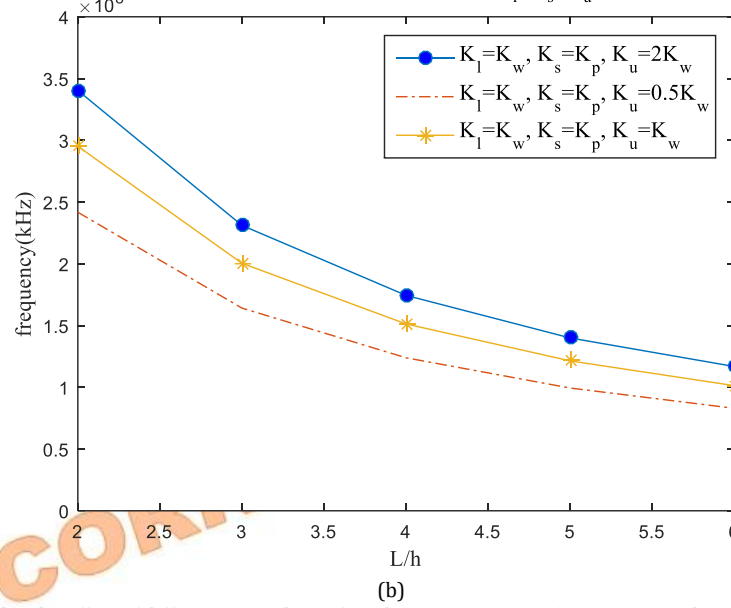

(b)

Fig. 13. (a, b) The effect of different Kerr elastic foundation parameters (K_l, K_s, K_u) on the natural frequency

This section presents the vibration of sandwich microbeams with different material porous cores and examines the influence of various temperature changes. Figure 14a and b illustrate the natural frequency of the sandwich microbeam for different temperature conditions. It can be observed that as the temperature of the microbeam increases, the natural frequency decreases, because the structure becomes softener. This demonstrates the crucial role temperature dependency plays in influencing the vibration behavior of microbeams through temperature changes. Also, it is shown that Si304 and SUS304 have the highest and lowest natural frequencies, respectively.

Properties of Porous Core at different temperatures

(a)

Effect of temprature to Natural Frequency
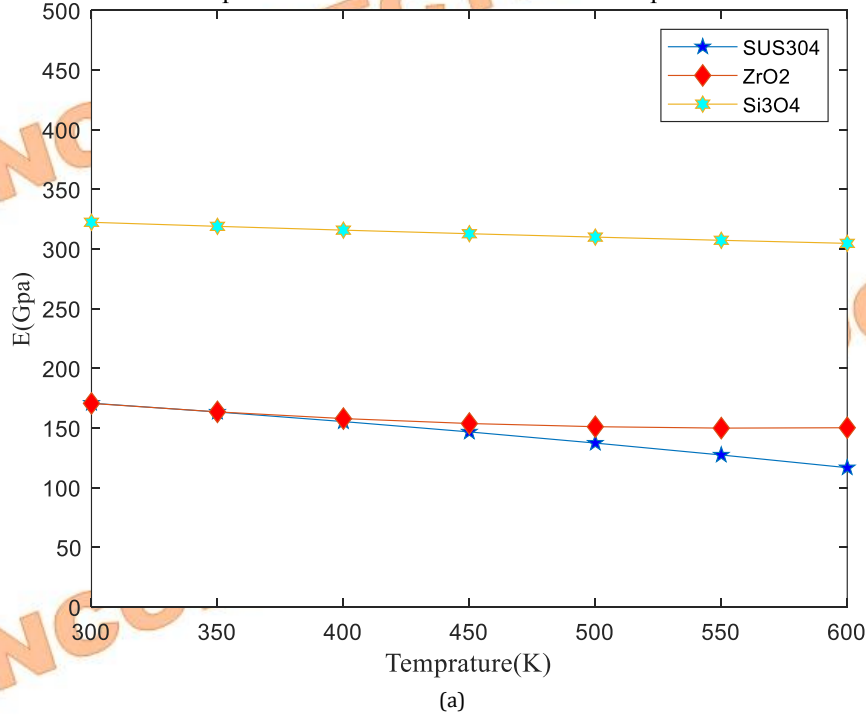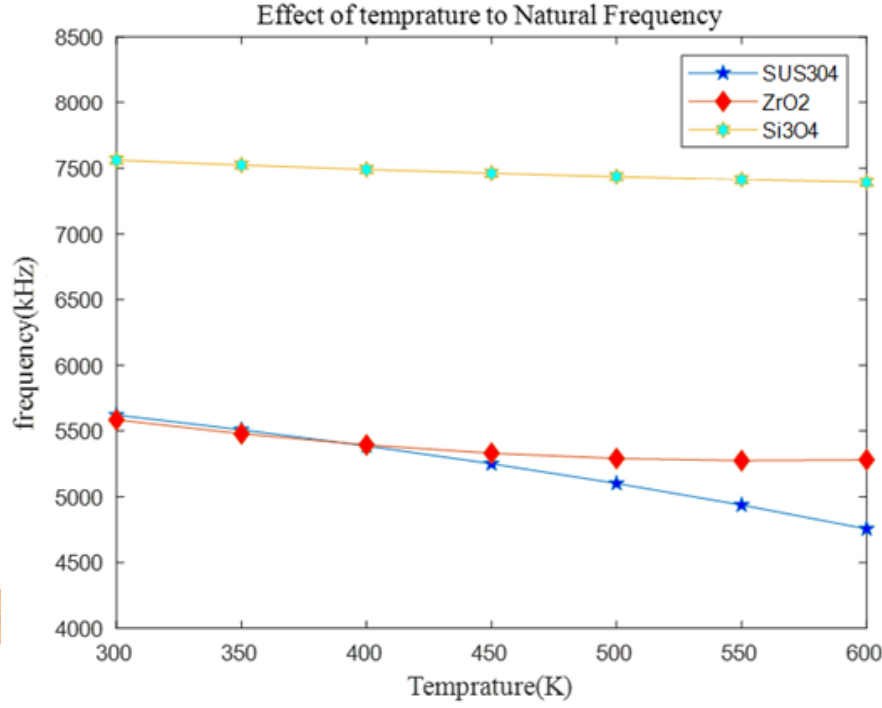
(b)

Fig. 14. (a, b) The effect of different material porous cores on the natural frequencies

There are many different theories for small-scale structures. The mechanical behavior of such micro-scale objects is not adequately modeled by the classical theories. In this section, the effect of size dependence on small scale on the natural frequencies of sandwich microbeams is investigated. These models include NSGT, SGT, NT, and MCST. As shown in Fig. 15, the comparison of the material small-scale parameter based on various theories and the classical theory on the natural frequency is investigated. Considering the small-scale characteristic parameters, NSGT and SGT have the same range of natural frequencies. The accuracy of NSGT and SGT was also compared with that of MCST and CT. As shown in this figure, the comparison results indicated that the reason for the difference between the frequencies predicted by the two higher-order theories NSGT, SGT, and classical theory can be easily illustrated by the additional material and non-local parameters in the constitutive equations of sandwich microbeams.

Comparison of the material length scale parameter to different theory and classical theory
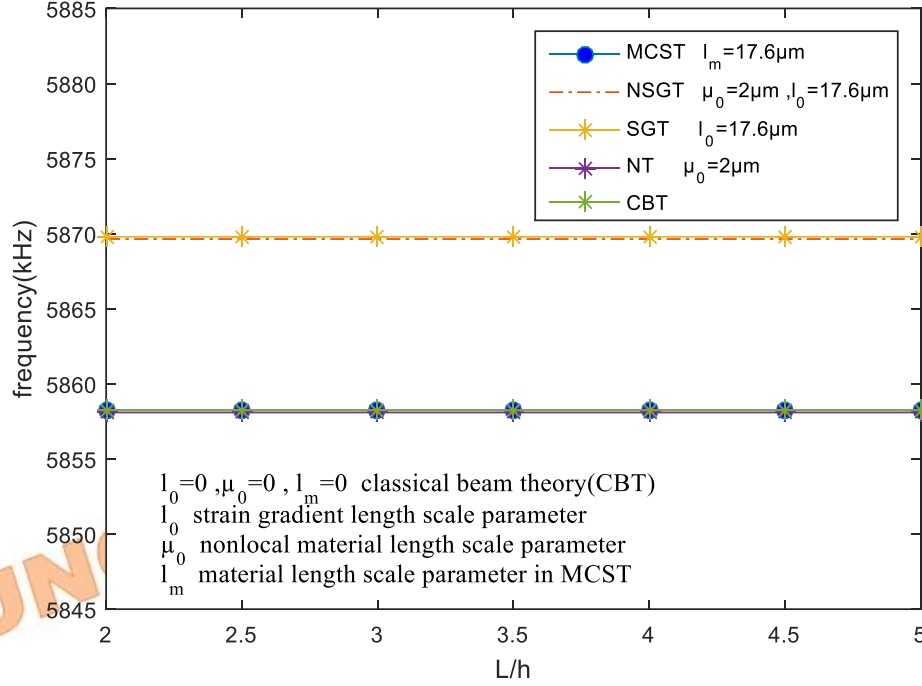

Fig. 15. Comparison of the material length scale parameter to different theories and classical theory on the natural frequency

6. Conclusions

The objective of this study is to investigate a vibration analysis of a sandwich microbeam for various reinforcements including GPLs, CNTs, and CNRs in the face sheet layers and different porous materials in the core using the shear and normal deformation beam theory (SNDBT), where the material properties are dependent to temperature. Also, to consider the size effect, the various small-scale theories including modified couple stress theory (MCST) and nonlocal strain gradient theory (NSGT) are investigated. These microbeams are placed on different elastic foundations including Kerr, Pasternak, and Winkler. This study makes a significant contribution to the realm of practical engineering applications by integrating insights from previous research for analyzing the vibration of porous FG beams with different elastic supports, Pasternak, Kerr, and Winkler elastic foundations, and different reinforcements. Additionally, this study incorporates various porosity distributions including asymmetric, symmetric, and uniform in the core for a sandwich microbeam. It also provides valuable results on the free vibration behavior of porous microbeams resting on elastic foundations. The results, both with and without thickness stretching, demonstrate that the shear and normal beam theory improves the results. The various parameters, including different size effect theories, porosity distribution, core-to-face sheet thickness ratio, axial wave number, aspect ratio, different temperatures, volume fractions of CNTs, and different reinforcements such as GPLs, CNTs, and CNRs, are investigated for their effect on the natural frequency of a sandwich microbeam. This comparison will allow for the selection of the most suitable reinforcements, taking into account both industry requirements and economic considerations. The most significant findings of this research are presented as follows:

1- Increasing the length-to-thickness ratio of a micro-sandwich beam results in a decrease in the natural frequency due to a reduction in stiffness. However, this phenomenon also leads to a softening of the structure.

2- The findings indicate that an increase in the strain gradient parameter results in an elevated frequency, which can be attributed to the enhanced stiffness of the microstructure. The influence of nonlocal parameters on the first four natural frequencies of a sandwich microbeam is illustrated. The findings demonstrate that the nonlocal parameters of the beam exert a greater influence on the high frequencies of sandwich microbeams than on the low frequencies. The results show that using nonlocal strain gradient theory can make a sandwich microbeam soften and stiffen. Small length scale parameters have a significant effect on the frequency, as shown by the increase in strain gradient and non-local parameters that it leads to increase and decrease the natural frequency, respectively.

3- It showed that for $\frac{L}{l_0} = 75$, with increasing of h_c from $0.5h$ to $0.9h$, the natural frequency decreases by 55%, because the structure becomes softer.

4- The findings indicate that the frequency of sandwich beams may be overestimated for L/h >

24

7 in the absence of thickness stretching. The shear and normal deformation beam theory can account for the thickness stretching effect and yield highly accurate results.

5- The results demonstrated the impact of various distributions of CNTs (FG-AV, FG-XX, FG-UU, FG-OO, and FG-VA) on the natural frequency. It was observed that FG-OO exhibited the lowest natural frequency, while FG-XX demonstrated the highest. Also, the stiffness and natural frequency of the structure change when different reinforcement distributions are used in the face sheet layer. The natural frequency increases by 67.4%, when FG-XX is compared to FG-UU face sheets. It decreases by 24.8% when FG-OO is compared to FG-UU.

6- The findings indicate that as the porosity coefficient of the core increases, the frequency of the beams tends to decrease. This phenomenon can be observed by comparing the natural frequency values of beams with different porosity distributions. As the distributions become more 2asymmetric, the natural frequency values tend to be higher, while for uniform distributions, the values tend to be lower.

7- The study showed how different reinforcements (such as GPL, CNT, and CNR) affect the frequency of a sandwich beam in the face sheet layer. The frequency of graphene platelets is displayed as the highest frequency, followed by carbon nanotubes and carbon nanorods, which have the lowest frequency. It can be seen that CNRs have relatively good strength, are made with low-cost materials, and can be considered a good alternative for nanocomposites in many industries. The sandwich beams are compared to those without reinforcement, by increasing the volume fraction of the reinforcements, the stiffness and the frequency of the sandwich microbeam increases. The GPLs increase the frequency by 10%, the CNTs by 7%, and the CNRs by 4%.

8- The results of the present study show that consideration of Pasternak's, Kerr's and Winkler's foundations leads to a significant increase in the frequencies for a microbeam, respectively.

9- The impact of shear layer stiffness (K_s) is more important, and it has more influence than other elastic foundation parameters. It was found that when the stiffness of the shear layer is increased, the frequency goes up. By making the springs (K_u, K_l), stiffer, a higher rise in the frequency of the microbeam is seen.

10- The frequency of the sandwich microbeam with different porous cores for various temperature conditions is illustrated. It can be observed that as the temperature increases, the frequency is reduced. Additionally, It can also be seen that the temperature dependence of the materials has a significant impact on the vibration stimulation.

11- The results demonstrated that NSGT and SGT exhibited identical ranges of natural frequency. The precision of NSGT and SGT was also evaluated in comparison to that of the classical theory. The findings revealed that the discrepancy between the frequencies predicted by the two higher order theories, NSGT and SGT, and the classical theory can be attributed to the inclusion of additional scale and nonlocal parameters in the constitutive equations.

Nomenclature

L	Length of micro beam	E_{CNT}	Elastic modulus of CNTs
u_0	Axial displacement	G_{CNT}	Shear modulus of CNTs
w_1, w_2	Shear and bending components of displacement	$E(z)$	Elastic modulus of porous Core
σ_{ij}	Stress components of sandwich micro beam	$G(z)$	Shear modulus of porous Core
ε_{kl}	Strain components of sandwich micro beam	$\rho(z)$	Mass density of porous Core
h_t	Thickness of top face sheet	e_0	Coefficients of porosity
h_b	Thickness of bottom face sheet	e_m	Coefficients of mass density
V_m	Volume fractions of matrix	I_0	Strain gradient length scale parameter

V_{CNT}	Volume fractions of CNTs	$\mu = (ea)^2$	Nonlocal parameter
ρ_f	The mass density of face layers	l_m	Material length scale parameter
υ_f	Poisson's ratio of face layers	χ_{ij}	Curvature tensor
ρ_m	The mass density of the matrix	$\mu(z)$	Lame's parameter
υ_m	Poisson's ratio of matrix	δT	Variation of kinetic energy
h	Thickness of sandwich beam	δU	Variation of strain energy

Conflicts of Interest

The author declares that there is no conflict of interest regarding the publication of this article.

Appendixes

Appendix A

The resultant forces and moments in Eqs. (26) are defined as follows:

$$N_x = \int \sigma_x dz$$
$$M_x = \int \sigma_x z dz$$
$$Q_x = \int \sigma_{xz} dz$$
$$f_x = \int \sigma_x z^2 dz$$
$$f_{xx} = \int \sigma_x z^3 dz$$
$$M_Z = \int \sigma_z z dz$$
$$g_x = \int \sigma_{xz} z^2 dz$$
$$M_{xy}^{(0)} = \int M_{xy} dz$$
$$M_{xy}^{(2)} = \int M_{xy} z^2 dz$$
$$M_{yz}^{(1)} = \int M_{yz} z dz$$

Appendix B

The variables in Eqs. (27)-(30) are defined as follows:

$$D^{(0)} = \int Q_{66} dz$$
$$D^{(1)} = \int Q_{66} z dz$$
$$D^{(2)} = \int Q_{66} z^2 dz$$
$$D^{(3)} = \int Q_{66} z^3 dz$$
$$D^{(4)} = \int Q_{66} z^4 dz$$
$$E^{(0)} = \int Q_{55} dz$$
$$E^{(1)} = \int Q_{55} z dz$$
$$E^{(2)} = \int Q_{55} z^2 dz$$
$$E^{(3)} = \int Q_{55} z^3 dz$$
$$E^{(4)} = \int Q_{55} z^4 dz$$
$$F^{(0)} = \int Q_{33} dz$$
$$F^{(1)} = \int Q_{33} z dz$$
$$F^{(2)} = \int Q_{33} z^2 dz$$
$$F^{(3)} = \int Q_{33} z^3 dz$$
$$F^{(4)} = \int Q_{33} z^4 dz$$
$$I_0 = \int \rho dz$$
$$I_1 = \int \rho z dz$$
$$I_2 = \int \rho z^2 dz$$
$$I_3 = \int \rho z^3 dz$$
$$I_f = \int \rho f dz$$
$$I_{ff} = \int \rho f^2 dz$$
$$I_{fz} = \int \rho f z dz$$
$$I_g = \int \rho g dz$$
$$I_{gg} = \int \rho g^2 dz$$

Appendix C

To find the elements of the stiffness matrix, substitute Eq. (31) into Eq. (27) through Eq. (30).

$$q = \frac{m\pi}{L}, \; l = l_0$$

$$K_{11} = -A^{(0)}q^2 - l^2 A^{(0)}q^4$$

$$K_{12} = A^{(1)}q^3 + l^2 A^{(1)}q^5$$

$$K_{13} = \frac{4A^{(3)}q^3}{3h^2} + \frac{4A^{(3)}l^2 q^5}{3h^2}$$

$$K_{14} = \frac{8B^{(1)}q}{h^2} + \frac{8B^{(1)}q^3 l^2}{3h^2}$$

$$K_{21} = A^{(1)}q^3 + l^2 A^{(1)}q^5$$

$$K_{22} = -A^{(2)}q^4 - l^2 A^{(2)}q^6 - \frac{C^{(0)}}{2}q^4 - \frac{C^{(0)}l^2 q^6}{2}$$

$$K_{23} = \frac{-4A^{(4)}q^4}{3h^2} - \frac{4l^2 A^{(4)}q^6}{3h^2} - \frac{C^{(2)}q^4}{h^2} - \frac{C^{(0)}q^4}{4} + \frac{C^{(2)}l^2 q^6}{h^2} - \frac{C^{(0)}l^2 q^6}{4}$$

$$K_{24} = \frac{8B^{(2)}q^2}{h^2} + \frac{8B^{(2)}q^4 l^2}{h^2} - \frac{C^{(0)}q^4}{4} + \frac{C^{(2)}q^4}{4} - \frac{C^{(0)}q^6 l^2}{4} + \frac{C^{(2)}l^2 q^6}{h^2}$$

$$K_{31} = \frac{4A^{(3)}q^3}{3h^2} + \frac{4l^2 A^{(3)}q^5}{3h^2}$$

$$K_{32} = -\frac{4A^{(4)}q^4}{3h^2} - \frac{4l^2 A^{(4)}q^6}{3h^2} - \frac{C^{(2)}q^4}{h^2} - \frac{C^{(0)}q^4}{4} - \frac{C^{(2)}l^2 q^6}{h^2} - \frac{C^{(0)}l^2 q^6}{4}$$

$$K_{33} = -\frac{16A^{(6)}q^4}{9h^4} - \frac{16l^2 A^{(6)}q^6}{9h^4} - \frac{16E^{(4)}q^2}{h^4} + \frac{4E^{(2)}q^2}{h^2} + \frac{16l^2 E^{(4)}q^4}{h^4} + \frac{4l^2 E^{(2)}q^4}{h^2} + \frac{4E^{(2)}q^2}{h^2} - E^{(0)}q^2 + \frac{4l^2 E^{(2)}q^4}{h^2} - E^{(0)}l^2 q^4 \\ -\frac{2C^{(4)}q^4}{h^4} - \frac{C^{(2)}q^4}{2h^2} - \frac{2C^{(4)}l^2 q^6}{h^4} - \frac{C^{(2)}l^2 q^6}{2h^2} - \frac{C^{(2)}q^4}{h^2} - \frac{C^{(2)}l^2 q^6}{h^2} - \frac{C^{(0)}q^4}{8} - \frac{C^{(0)}l^2 q^6}{8} + \frac{8C^{(2)}q^2}{h^2} + \frac{8C^{(2)}l^2 q^4}{h^2}$$

$$K_{34} = \frac{32B^{(4)}q^2}{3h^4} + \frac{32B^{(4)}l^2 q^4}{3h^4} + \frac{4E^{(2)}q^2}{h^2} - \frac{16E^{(4)}q^2}{h^4} + \frac{4E^{(2)}l^2 q^4}{h^2} - \frac{16E^{(4)}l^2 q^4}{h^4} - E^{(0)}q^2 + \frac{4E^{(2)}q^2}{h^2} - E^{(0)}l^2 q^4 + \frac{4E^{(2)}l^2 q^4}{h^2} \\ -\frac{C^{(2)}q^4}{2h^2} + \frac{2C^{(4)}q^4}{h^4} - \frac{l^2 C^{(2)}q^6}{2h^2} + \frac{2l^2 C^{(4)}q^6}{h^4} - \frac{C^{(0)}q^4}{8} + \frac{C^{(2)}q^4}{2h^2} - \frac{l^2 C^{(0)}q^6}{8} + \frac{l^2 C^{(2)}q^6}{2h^2} + \frac{8C^{(2)}q^2}{h^2} + \frac{8l^2 C^{(2)}q^2}{h^2}$$

$$K_{41} = -\frac{8B^{(1)}q}{h^2} - \frac{8B^{(1)}q^3 l^2}{h^2}$$

$$K_{42} = \frac{8B^{(2)}q^2}{h^2} + \frac{8B^{(2)}q^4 l^2}{h^2} - \frac{C^{(0)}q^4}{4} - \frac{l^2 C^{(0)}q^6}{4} + \frac{C^{(2)}q^4}{h^2} + \frac{C^{(2)}l^2 q^6}{h^2}$$

$$K_{43} = \frac{32B^{(4)}q^2}{3h^4} + \frac{32B^{(4)}q^4 l^2}{3h^4} + \frac{4E^{(2)}q^2}{h^2} - \frac{16E^{(4)}q^2}{h^4} + \frac{4E^{(2)}l^2 q^4}{h^2} - \frac{16E^{(4)}l^2 q^4}{h^4} - E^{(0)}q^2 + \frac{4E^{(2)}q^2}{h^2} - E^{(0)}l^2 q^4 + \frac{4E^{(2)}l^2 q^4}{h^2} \\ -\frac{C^{(2)}q^4}{2h^2} + \frac{2C^{(4)}q^4}{h^4} - \frac{C^{(2)}l^2 q^6}{2h^2} + \frac{2C^{(4)}l^2 q^6}{h^4} - \frac{C^{(0)}q^4}{8} + \frac{C^{(2)}q^4}{2h^2} - \frac{C^{(0)}l^2 q^6}{8} + \frac{C^{(2)}l^2 q^6}{2h^2} + \frac{8C^{(2)}q^2}{h^4} + \frac{8C^{(2)}l^2 q^4}{h^4}$$

$$K_{44} = -\frac{64F^{(2)}}{h^4} - \frac{64l^2 F^{(2)}q^2}{h^4} - E^{(0)}q^2 + \frac{4E^{(2)}q^2}{h^2} - E^{(0)}l^2 q^4 + \frac{4E^{(2)}l^2 q^4}{h^2} \\ +\frac{4E^{(2)}q^2}{h^2} - \frac{16E^{(4)}q^2}{h^4} + \frac{4E^{(2)}l^2 q^4}{h^2} - \frac{16E^{(4)}l^2 q^4}{h^4} - \frac{C_0 q^4}{8} + \frac{C_2 q^4}{8} - \frac{C_0 l^2 q^6}{8} \\ +\frac{C_2 l^2 q^6}{2h^2} + \frac{C_2 q^4}{2h^2} - \frac{2C_4 q^4}{h^4} + \frac{C_2 l^2 q^6}{2h^2} + \frac{2C_4 l^2 q^6}{h^4} - \frac{8C_2 q^2}{h^4} - \frac{8C_2 l^2 q^4}{h^4}$$

27

Appendix D

By substituting Eqs. (31) into Eqs. (27)-(30), the elements of the mass matrix are derived as follows:

$$\mu^2 = (ea)^2$$
$$M_{11} = -I_0 - \mu^2 I_0 q^2$$
$$M_{12} = I_1 q + \mu^2 I_1 q^3$$
$$M_{13} = -I_f q - \mu^2 I_f q^3$$
$$M_{14} = 0$$
$$M_{21} = I_1 q + \mu^2 I_1 q^3$$
$$M_{22} = I_2 q^2 - I_0 + \mu^2 I_2 q^4 - \mu^2 I_0 q^2$$
$$M_{23} = I_{fz} q^2 - I_0 + \mu^2 I_{fz} q^4 - \mu^2 I_0 q^2$$
$$M_{24} = -I_g - \mu^2 I_g q^2$$
$$M_{31} = -I_f q - \mu^2 I_f q^3$$
$$M_{32=} +I_{fz} q^2 - I_0 - \mu^2 I_{fz} q^4 + \mu^2 I_0 q^2$$
$$M_{33} = -I_{ff} q^2 - \mu^2 I_{ff} q^4 - \mu^2 I_0 q^2 - I_0$$
$$M_{34} = -I_g - \mu^2 I_g q^2$$
$$M_{41} = 0$$
$$M_{42} = -I_g - \mu^2 I_g q^2$$
$$M_{43} = -I_g - \mu^2 I_g q^2$$
$$M_{44} = -I_{gg} - \mu^2 I_{gg} q^2$$

References

[1] Kheirikhah, M., Ghiasvand, M., Gohari, S. and Burvill, C., 2023. Free vibration analysis of composite sandwich beams reinforced by functionally graded graphene nanoplatelets. *Mechanics of Composite Materials, 59*(5), pp. 959-976.

[2] Arshid, E., Amir, S. and Loghman, A., 2024. Aero-hygro-thermoelastic size-dependent analysis of ncmf-reinforced gnps sector microplates located between piezoelectric patches in supersonic flow considering surface stress effects. *Mechanics Based Design of Structures and Machines, 52*(9), pp. 6911-6972.

[3] Mohammadimehr, M., Mehrabi, M. and Mousavinejad, F.S., 2021. Magneto-mechanical vibration analysis of single-/three-layered micro-timoshenko porous beam and graphene platelet as reinforcement based on modified strain gradient theory and differential quadrature method. *Journal of Vibration and Control, 27*(15-16), pp. 1842-1859.

[4] Adiyaman, G., 2024. Free vibration analysis of a porous 2d functionally graded beam using a high-order shear deformation theory. *Journal of Vibration Engineering and Technologies, 12*(2), pp. 2499-2516.

[5] Khakpour, M., Bazargan-Lari, Y., Zahedinejad, P. and Kazemzadeh-Parsi, M.-J., 2022. Vibrations evaluation of functionally graded porous beams in thermal surroundings by generalized differential quadrature method. *Shock and Vibration, 2022*(1), pp. 8516971.

[6] Marandi, S.M. and Karimipour, I., 2023. Free vibration analysis of a nanoscale FG-CNTRCs sandwich beam with flexible core: Implementing an extended high order approach. *Engineering Structures, 276*, p. 115320.

[7] Mohamed, I., Kahya, V. and Şimşek, S., 2024. A new higher-order finite element model for free vibration and buckling of functionally graded sandwich beams with porous core resting on a two-parameter elastic foundation using quasi-3d theory. *Iranian Journal of Science and Technology, Transactions of Civil Engineering*, *2024*, pp. 1-26.

[8] Zhang, L., Xu, Z., Gao, M., Xu, R. and Wang, G., 2023. Static, dynamic and buckling responses of random functionally graded beams reinforced by graphene platelets. *Engineering Structures, 291*, p. 116476.

[9] Alibar, M.Y., Safaei, B., Asmael, M. and Zeeshan, Q., 2021. Effect of carbon nanotubes and porosity on vibrational behavior of nanocomposite structures: A review. *Archives of Computational Methods in Engineering*, 2021, pp. 1-37.

[10] Zamani, H., 2021. Frequency analysis of fg-cnt–reinforced composite doubly curved panels on visco-pasternak medium. *Advanced Composites and Hybrid Materials, 4*, pp. 830-844.

[11] Wu, Z., Zhang, Y. and Yao, G., 2023. Natural frequency and stability analysis of axially moving functionally graded carbon nanotube-reinforced composite thin plates. *Acta Mechanica, 234*(3), pp. 1009-1031.

[12] Safaei, M., Malekzadeh, P. and Haghighi, M.G., 2024. Out-of-plane moving load response and vibrational behavior of sandwich curved beams with gplrc face sheets and porous core. *Composite Structures, 327*, p. 117658.

[13] Noruzi, A., Mohammadimehr, M. and Bargozini, F., 2024. Experimental free vibration and tensile test results of a five-layer sandwich plate by comparing various carbon nanostructure reinforcements with sma. *Heliyon, 10*(10), e31164.

[14] Bargozini, F. and Mohammadimehr, M., 2024. The theoretical and experimental buckling analysis of a nanocomposite beams reinforced by nanorods made of recycled materials. *Polymer Composites, 45*(4), pp. 3327-3342.

[15] Ghorbanpour Arani, A., Babaakbar-Zarei, H., Pourmousa, P. and Eskandari, M., 2018. Investigation of free vibration response of smart sandwich micro-beam on winkler–pasternak substrate exposed to multi physical fields. *Microsystem Technologies, 24*, pp. 3045-3060.

[16] Bamdad, M., Mohammadimehr, M. and Alambeigi, K., 2019. Analysis of sandwich timoshenko porous beam with temperature-dependent material properties: Magneto-electro-elastic vibration and buckling solution. *Journal of Vibration and Control, 25*(23-24), pp. 2875-2893.

[17] Rahmani, O., Shokrnia, M., Golmohammadi, H. and Hosseini, S., 2018. Dynamic response of a single-walled carbon nanotube under a moving harmonic load by considering modified nonlocal elasticity theory. *The European Physical Journal Plus, 133*, pp. 1-13.

[18] Zenkour, A., 2018. Nonlocal elasticity and shear deformation effects on thermal buckling of a cnt embedded in a viscoelastic medium. *The European Physical Journal Plus, 133*(5), pp. 196.

[19] Jena, S.K., Chakraverty, S. and Malikan, M., 2020. Vibration and buckling characteristics of nonlocal beam placed in a magnetic field embedded in winkler–pasternak elastic foundation using a new refined beam theory: An analytical approach. *The European Physical Journal Plus, 135*(2), pp. 1-18.

[20] Jena, S.K., Chakraverty, S., Mahesh, V., Harursampath, D. and Sedighi, H.M., 2022. Free vibration of functionally graded beam embedded in winkler-pasternak elastic foundation with geometrical uncertainties using symmetric gaussian fuzzy number. *The European Physical Journal Plus, 137* (3), p. 399.

[21] Bidgoli, E.M.-R. and Arefi, M., 2023. Effect of porosity and characteristics of carbon nanotube on the nonlinear characteristics of a simply-supported sandwich plate. *Archives of Civil and Mechanical Engineering, 23*(3), p. 214.

[22] Priyanka, R. and Pitchaimani, J., 2022. Static stability and free vibration characteristics of a micro laminated beam under varying axial load using modified couple stress theory and ritz method. *Composite Structures, 281*, p. 115028.

[23] Hosseini, S.A., Hamidi, B.A. and Maboudi, G., 2022. On new nonlinearity in third-order elastic modulus for vibrational analysis of fg porous beam based on nonlocal strain gradient and surface energy by modified

homotopy perturbation method. *The European Physical Journal Plus, 137*(4), pp. 1-18.

[24] Ramteke, P.M. and Panda, S.K., 2023. Computational modelling and experimental challenges of linear and nonlinear analysis of porous graded structure: A comprehensive review. *Archives of Computational Methods in Engineering, 30*(5), pp. 3437-3452.

[25] Li, S., Zheng, W. and Li, L., 2024, Spatiotemporally nonlocal homogenization method for viscoelastic porous metamaterial structures, *International Journal of Mechanical Sciences,* 282, p. 109572.

[26] Li, S. and Li, L., 2024, A homogenization method incorporating surface effect for thin metamaterial structure. *International Journal of Engineering Science*, *201*, p. 104093.

[27] Dehkordi, H.R.B. and Beni, Y.T., 2023. Size-dependent coupled bending-torsional vibration of functionally graded carbon nanotube reinforced composite timoshenko microbeams. *Archives of Civil and Mechanical Engineering, 23*(3), p. 186.

[28] Mehralian, F., Beni, Y.T. and Zeverdejani, M.K., 2017. Nonlocal strain gradient theory calibration using molecular dynamics simulation based on small scale vibration of nanotubes. *Physica B: Condensed Matter, 514*, pp. 61-69.

[29] Li, R., Li, L. and Jiang Y., 2025, A physics-based nonlocal theory for particle-reinforced polymer composites. *Journal of Mechanical Sciences*, 285, p. 109800.

[30] Mohammadian, M., 2022. Application of the modified fourier series method and the genetic algorithm for calibration of small-scale parameters in the nonlocal strain gradient nanobeams. *Mathematical Methods in the Applied Sciences, 45*(10), pp. 6325-6345.

[31] Eroğlu, M., Esen, İ. and Koç, M.A., 2024. Thermal vibration and buckling analysis of magneto-electro-elastic functionally graded porous higher-order nanobeams using nonlocal strain gradient theory. *Acta Mechanica, 235*(2), pp. 1175-1211.

[32] Nuhu, A.A. and Safaei, B., 2023. On the advances of computational nonclassical continuum theories of elasticity for bending analyses of small-sized plate-based structures: A review. *Archives of Computational Methods in Engineering, 30*(5), pp. 2959-3029.

[33] Fatahi, M.H., Hamedi, M. and Safarabadi, M., 2021. Experimental and numerical implementation of auxetic substrate for

enhancing voltage of piezoelectric sandwich beam harvester. *Mechanics of Advanced Materials and Structures, 29*(27)**,** pp. 6107-6117.

[34] Mohammadi, M., Safarabadi, M., Rastgoo, A. and Farajpour, A., 2016. Hygro-mechanical vibration analysis of a rotating viscoelastic nanobeam embedded in a visco-pasternak elastic medium and in a nonlinear thermal environment. *Acta Mechanica, 227***,** pp. 2207-2232.

[35] Safarabadi, M., Mohammadi, M., Farajpour, A. and Goodarzi, M., 2015. Effect of surface energy on the vibration analysis of rotating nanobeam. *Journal of Solid Mechanics, 7*(3), pp. 299-311.

[36] Li, L., Li, X. and Yu, Y., 2016. Free vibration analysis of nonlocal strain gradient beams made of functionally graded material. I*nternational Journal of Engineering Science*, 102, pp. 77-92.

[37] Qian, Q., Zhu, F., Fan, Y., Hang, Z., Feng, C. and Yang, J., 2023. Parametric study on nonlinear vibration of FG-GNPRC dielectric beam with kelvin–voigt damping. *Thin-Walled Structures, 185***,** p. 110617.

[38] Asgari, M., Mohammadimehr, M., Arabzadeh-Ziari, M. and Arabzadeh-Ziari, E., 2024. Static bending, vibration, and buckling responses of a sandwich beam composed of five layers considering honeycomb core and CNTRC with sma particles and temperature-dependent material properties using SSDT. *Mechanics of Advanced Composite Structures*, *12*(1), pp. 153-168.

[39] Brijeshgangil, B., Bharadvaj, M. and Yadav, J., 2024. Thermo-mechanical and wear properties of natural fibre-reinforced epoxy composites for structural applications. *Mechanics of Advanced Composite Structures*, *12*(1), pp. 141-152.

[40] Ni, Z., Zhu, F., Fan, Y., Yang, J., Hang, Z. and Feng, C., 2023. Numerical study on damped nonlinear dynamics of cracked fg-gnprc dielectric beam with active tuning. *Thin-Walled Structures, 192***,** p. 111122.

[41] Hang, Z., Ni, Z., Yang, J., Fan, Y., Feng, C. and Wang, S., 2024, Nonlinear vibration of FG-GNPRC dielectric beam with kelvin-voigt damping in thermal environment. *International Journal of Structural Stability and Dynamics*, 24(12), p. 2450130.

[42] Jafari, M., Mohammadimehr, M., 2025, Forced vibration control of Timoshenko's micro sandwich beam with CNT/GPL/CNR reinforced composites integrated by piezoelectric on Kerr's elastic foundation using MCST, Journal of Computational Applied Mechanics 56 (1), 15-42.

[43] Jafari, M., Mohammadimehr, M., 2024, Active control for higher order micro sandwich beam with various cores integrated by piezoelectric layers based on MSGT on the Pasternak foundation, Journal of Vibration and Control, 10775463241291126.

[44] Motalebi, V., Mohammadimehr, M., Bargozini, F., Vibration response of sandwich plate reinforced by GPLs/GOAM, Mechanics Research Communications 141, 104334

[45] Nguyen, N.-D., Nguyen, T.-K., Thai, H.-T. and Vo, T.P., 2018. A ritz type solution with exponential trial functions for laminated composite beams based on the modified couple stress theory. *Composite Structures, 191***,** pp. 154-167.

[46] Shariati, M., Shishesaz, M., Sahbafar, H., Pourabdy, M. and Hosseini, M., 2021. A review on stress-driven nonlocal elasticity theory. *Journal of Computational Applied Mechanics, 52* (3)**,** pp. 535-552.

[47] Chen, D., Wang, Y., Zheng, S., Liang, Y. and Sun, S., 2024. Isogeometric analysis of bi-directional functionally graded porous micro-beam with geometrical imperfections using nonlocal strain gradient theory. *Journal of Vibration Engineering and Technologies***,** *2024*, pp. 1-13.

[48] Lim, C., 2010. On the truth of nanoscale for nanobeams based on nonlocal elastic stress field theory: Equilibrium, governing equation and static deflection. *Applied Mathematics and Mechanics, 31*(1)**,** pp. 37-54.

[49] Ghayesh, M.H. and Farajpour, A., 2019. A review on the mechanics of functionally graded nanoscale and microscale structures. *International Journal of Engineering Science, 137***,** pp. 8-36.

[50] Sahmani, S., Aghdam, M.M. and Rabczuk, T., 2018. Nonlinear bending of functionally graded porous micro/nano-beams reinforced with graphene platelets based upon nonlocal strain gradient theory. *Composite Structures, 186***,** pp. 68-78.

[51] Faghidian, S.A., 2021. Contribution of nonlocal integral elasticity to modified strain gradient theory. *The European Physical Journal Plus, 136* (5)**,** p. 559.

[52] Iijima, S., 1991. Helical microtubules of graphitic carbon. *Nature, 354* (6348)**,** pp. 56-58.

[53] Mohammadimehr, M., Okhravi, S. and Akhavan Alavi, S., 2018. Free vibration analysis of magneto-electro-elastic cylindrical composite panel reinforced by various distributions of cnts with considering open and closed circuits

boundary conditions based on fsdt. *Journal of Vibration and Control, 24*(8)**,** pp. 1551-1569.

[54] Eghbali, M. and Hosseini, S.A., 2023. On moving harmonic load and dynamic response of carbon nanotube-reinforced composite beams using higher-order shear deformation theories. *Mechanics of Advanced Composite Structures, 10* (2)**,** pp. 257-270.

[55] Jooybar, N., Malekzadeh, P. and Fiouz, A., 2016. Vibration of functionally graded carbon nanotubes reinforced composite truncated conical panels with elastically restrained against rotation edges in thermal environment. *Composites Part B: Engineering, 106***,** pp. 242-261.

[56] Xu, Z. and Huang, Q., 2019. Vibro-acoustic analysis of functionally graded graphene-reinforced nanocomposite laminated plates under thermal-mechanical loads. *Engineering Structures, 186***,** pp. 345-355.

[57] Amir, S., Soleimani-Javid, Z. and Arshid, E., 2019. Size-dependent free vibration of sandwich micro beam with porous core subjected to thermal load based on ssdbt. *ZAMM-Journal of Applied Mathematics and Mechanics/Zeitschrift für Angewandte Mathematik und Mechanik, 99*(9)**,** p. e201800334.

[58] Mirjavadi, S.S., Mohasel Afshari, B., Shafiei, N., Rabby, S. and Kazemi, M., 2018. Effect of temperature and porosity on the vibration behavior of two-dimensional functionally graded micro-scale timoshenko beam. *Journal of Vibration and Control, 24*(18)**,** pp. 4211-4225.

[59] Touloukian, Y., Powell, R., Ho, C. and Nicolaou, M. 1974. Thermophysical properties of matter, the tprc data series. Volume 10. Thermal diffusivity. Data book. Purdue Univ., Lafayette, IN (USA). Thermophysical and Electronic Properties.

[60] Joueid, N., Zghal, S., Chrigui, M. and Dammak, F., 2023. Thermoelastic buckling analysis of plates and shells of temperature and porosity dependent functionally graded materials. *Mechanics of Time-Dependent Materials***,** 2023, pp. 1-43.

[61] Safari, M., Mohammadimehr, M. and Ashrafi, H., 2021. Free vibration of electro-magneto-thermo sandwich timoshenko beam made of porous core and GPLRC. *Advanced Nano Research, 10*(2)**,** pp. 115-128.